AD-A041 621 TEXAS UNIV AT AUSTIN APPLIED RESEARCH LABS F/G 20/1
UNDERWATER ACOUSTIC BACKSCATTERING AND ECHO STRUCTURE CHARACTER--ETC(U)
MAY 77 K W ALKIER N00024-75-C-6078
UNCLASSIFIED ARL-TR-77-28 NL

1 OF 1
ADA041621

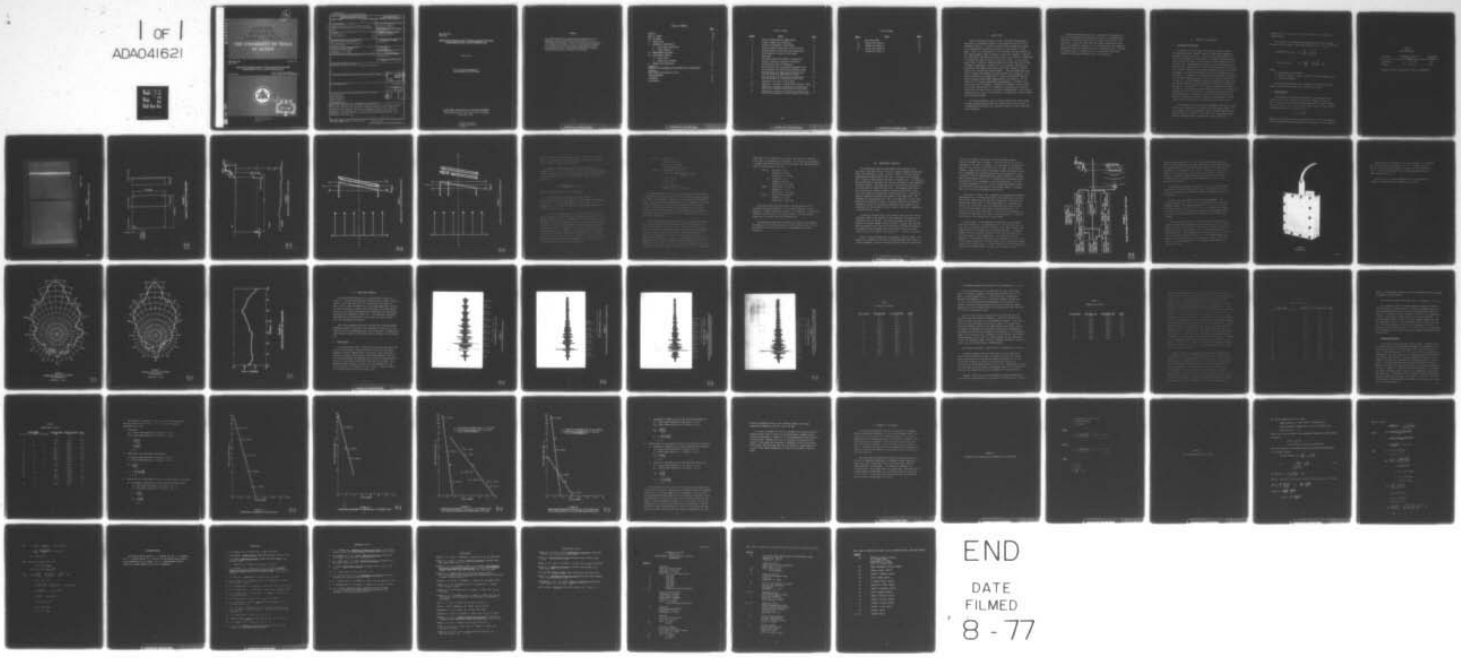

END

DATE FILMED
8 - 77

(12)

APPLIED RESEARCH LABORATORIES

THE UNIVERSITY OF TEXAS AT AUSTIN

ARL-TR-77-28
16 May 1977

Copy No. 31

UNDERWATER ACOUSTIC BACKSCATTERING AND ECHO STRUCTURE CHARACTERISTICS FOR A THIN STIFFENED PLATE

Klaus W. Alkier

NAVAL SEA SYSTEMS COMMAND
Contract N00024-75-C-6078, Item 0004

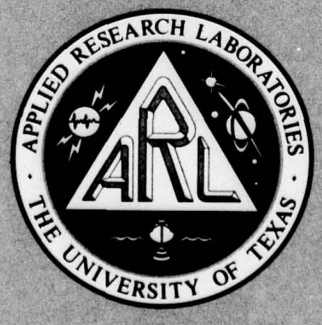

UNCLASSIFIED

SECURITY CLASSIFICATION OF THIS PAGE *(When Data Entered)*

REPORT DOCUMENTATION PAGE

READ INSTRUCTIONS BEFORE COMPLETING FORM

1. REPORT NUMBER	2. GOVT ACCESSION NO. / 3. RECIPIENT'S CATALOG NUMBER
4. TITLE *(and Subtitle)*: UNDERWATER ACOUSTIC BACKSCATTERING AND ECHO STRUCTURE CHARACTERISTICS FOR A THIN STIFFENED PLATE	5. TYPE OF REPORT & PERIOD COVERED: technical report
	6. PERFORMING ORG. REPORT NUMBER: ARL-TR-77-28
7. AUTHOR(s): Klaus W. Alkier	8. CONTRACT OR GRANT NUMBER(s): N00024-75-C-6078
9. PERFORMING ORGANIZATION NAME AND ADDRESS: Applied Research Laboratories, The University of Texas at Austin, Austin, TX 78712	10. PROGRAM ELEMENT, PROJECT, TASK AREA & WORK UNIT NUMBERS: Item 0004
11. CONTROLLING OFFICE NAME AND ADDRESS: Naval Sea Systems Command, Department of the Navy, Washington, D. C. 20362	12. REPORT DATE: 16 May 1977 13. NUMBER OF PAGES: 65
14. MONITORING AGENCY NAME & ADDRESS *(if different from Controlling Office)*	15. SECURITY CLASS. *(of this report)*: UNCLASSIFIED 15a. DECLASSIFICATION/DOWNGRADING SCHEDULE

16. DISTRIBUTION STATEMENT *(of this Report)*
Approved for public release; distribution unlimited.

17. DISTRIBUTION STATEMENT *(of the abstract entered in Block 20, if different from Report)*

ACCESSION for
NTIS White Section
DDC Buff Section
UNANNOUNCED
JUSTIFICATION
BY
DISTRIBUTION/AVAILABILITY CODES
Dist. AVAIL. and/or SPECIAL
A

18. SUPPLEMENTARY NOTES

19. KEY WORDS *(Continue on reverse side if necessary and identify by block number)*
backscattering
echo structure
reinforcing ribs
model studies
stiffened plates

20. ABSTRACT *(Continue on reverse side if necessary and identify by block number)*
This report describes an experimental investigation of the underwater acoustic reflection characteristics of a thin stiffened aluminum plate. Based on ray theory and echo structure analysis, an attempt was made to show that the presence of a reinforcing rib can be acoustically predicted in time. Good agreement between theoretically predicted and experimentally measured echo components was achieved.

404434

DD FORM 1 JAN 73 1473 EDITION OF 1 NOV 65 IS OBSOLETE

UNCLASSIFIED

SECURITY CLASSIFICATION OF THIS PAGE *(When Data Entered)*

ARL-TR-77-28
16 May 1977

UNDERWATER ACOUSTIC BACKSCATTERING AND ECHO STRUCTURE CHARACTERISTICS FOR A THIN STIFFENED PLATE

Klaus W. Alkier

NAVAL SEA SYSTEMS COMMAND
Contract N00024-75-C-6078, Item 0004

APPLIED RESEARCH LABORATORIES
THE UNIVERSITY OF TEXAS AT AUSTIN
AUSTIN, TEXAS 78712

ABSTRACT

This report describes an experimental investigation of the underwater acoustic reflection characteristics of a thin stiffened aluminum plate. Based on ray theory and echo structure analysis, an attempt was made to show that the presence of a reinforcing rib can be acoustically predicted in time. Good agreement between theoretically predicted and experimentally measured echo components was achieved.

TABLE OF CONTENTS

LIST OF FIGURES

LIST OF TABLES

I. INTRODUCTION

Acoustic scattering phenomena and echo structure characteristics have been of considerable interest to many researchers in the field of underwater acoustics. A summary by Horton[1] gives an extensive overview of the theoretical and practical work done in these topics in recent years. Most of the work reported in the literature has been confined to the simple geometric shapes of spheres, plates, and cylinders. Rayleigh[2] and later Morse[3] were perhaps the earliest and most widely known researchers to consider the rigid and elastic sphere and cylinder. In more recent times, Faran's[4] paper on scattering effects of a plane wave by an elastic cylinder is significant. Bowman et al.[5] list detailed scattering and directivity characteristics for many simple target shapes but fail to discuss echo structure and target strength. Franz and Deppermann[6] were first to suggest the presence of surface guided stress waves and called them Kriechwellen or creeping waves.[7] Barnard and McKinney[8] were the first to report similar waves experimentally, and Diercks et al.[9] and Horton et al.[10] further investigated the phenomena of scattering from thin walled elastic cylinders. Goldsberry[11] undertook a detailed study to show that the presence of an interface or discontinuity in density, in the form of a narrow slot or air gap cut longitudinally in the circumferential path of an air filled cylinder, can be predicted in time through echo structure analysis.

This study attempts to show in similar fashion that, with the help of these internally guided waves, the presence and location in time of a reinforcing rib placed in the acoustical shadow of a thin finite plate can be predicted.

Following well-known principles of ray theory, the assumption is made that these guided waves are being reflected at discontinuities and interfaces and are being refracted in accordance with Snell's law of refraction. Calculated travel times for several assumed travel paths and for two different locations of the reinforcing ribs are compared to measured values in the longitudinal mode of propagation only. No shear or flexural modes of vibration could be discerned with the target dimensions and driving frequency used in the experiment.

II. THEORETICAL CALCULATIONS

A. Sound Speed Calculations

To determine the sound speed in the target, one may consider that generally several different types of stress waves propagate in isotropic, elastic thin plates. No uniform terminology seems to be used in the literature; in this report the seemingly dominant and most easily excited wave types in these plates are called longitudinal and flexural waves. The propagation velocity of the longitudinal wave is generally much greater than the flexural wave, and usually, for a given set of physical dimensions and driving frequency,[12] one of the two will be dominant. The term thin refers to the ratio of thickness to the wavelength. The targets in this experiment are considered thin because, for the signal frequency used, the ratio of thickness to wavelength[13] is $d/\lambda=0.03$. As the wavelength increases and approaches a value twice the lateral dimensions, the longitudinal and flexural wave velocities approach the same value.[14,15] This change in propagation velocity is not known to occur abruptly at some wavelength; rather it is gradual and continuous as either the frequency or the physical dimensions of the medium are varied. In general, the result is that one encounters in practice a combination of modes of stress wave propagation. However, it may not always be possible to identify each mode individually.

In most cases, one may express the propagation velocities of these waves by some combination of Poisson's ratio and Young's modulus. It is of interest here to note that the value for Young's modulus[16] and Poisson's ratio is usually[17,18] given only to one significant figure. These are tabulated values determined for static conditions; for

dynamic conditions, more accurate values would have to be determined experimentally.

The relations for determining the propagation velocities in thin plates for the two types of waves mentioned above are as follows.[19,20,21,22]

$$\text{longitudinal velocity} \qquad C_L = \sqrt{\frac{E}{\rho_m}} \sqrt{\frac{1}{1 - \nu^2}} \quad ,$$

$$\text{flexural velocity} \qquad C_F = \sqrt[4]{\frac{E}{\rho_m}} \sqrt[4]{\frac{\kappa^2}{1 - \nu^2}} \sqrt{\omega} \quad ,$$

where

ρ_m = mass density of the plate,
κ = radius of gyration, which is $\underline{a}/\sqrt{12}$ for plate thickness $\underline{a}$, and
ω = circular frequency.

The calculated values for these propagation velocities and travel times in type 6061-T6 aluminum alloys are given in Table I.

B. Target Geometry

If one assumes an acoustic plane wavefront for the targets shown in Figs. 1 and 2 and considers the geometrical arrangement shown in Fig. 3, then one may also assume acoustic travel paths within the plates, as shown in Figs. 4 and 5. The critical angle θ_c shown in these figures is defined by Snell's law of refraction as

$$\theta_c = \sin^{-1} \frac{C_1}{C_2} \quad ,$$

where C_1 is the sound velocity in the water, and C_2 is the sound velocity (in the longitudinal mode of propagation) in the plate. At this critical

TABLE I

WAVE VELOCITIES

Wave Type	Propagation Velocity m/sec	Travel Time μsec/m
Longitudinal	$C_L \approx 5.45 \times 10^3$	183.1
Flexural	$C_F \approx 1.37 \times 10^3$	728.4

Details for these calculations are given in Appendix A.

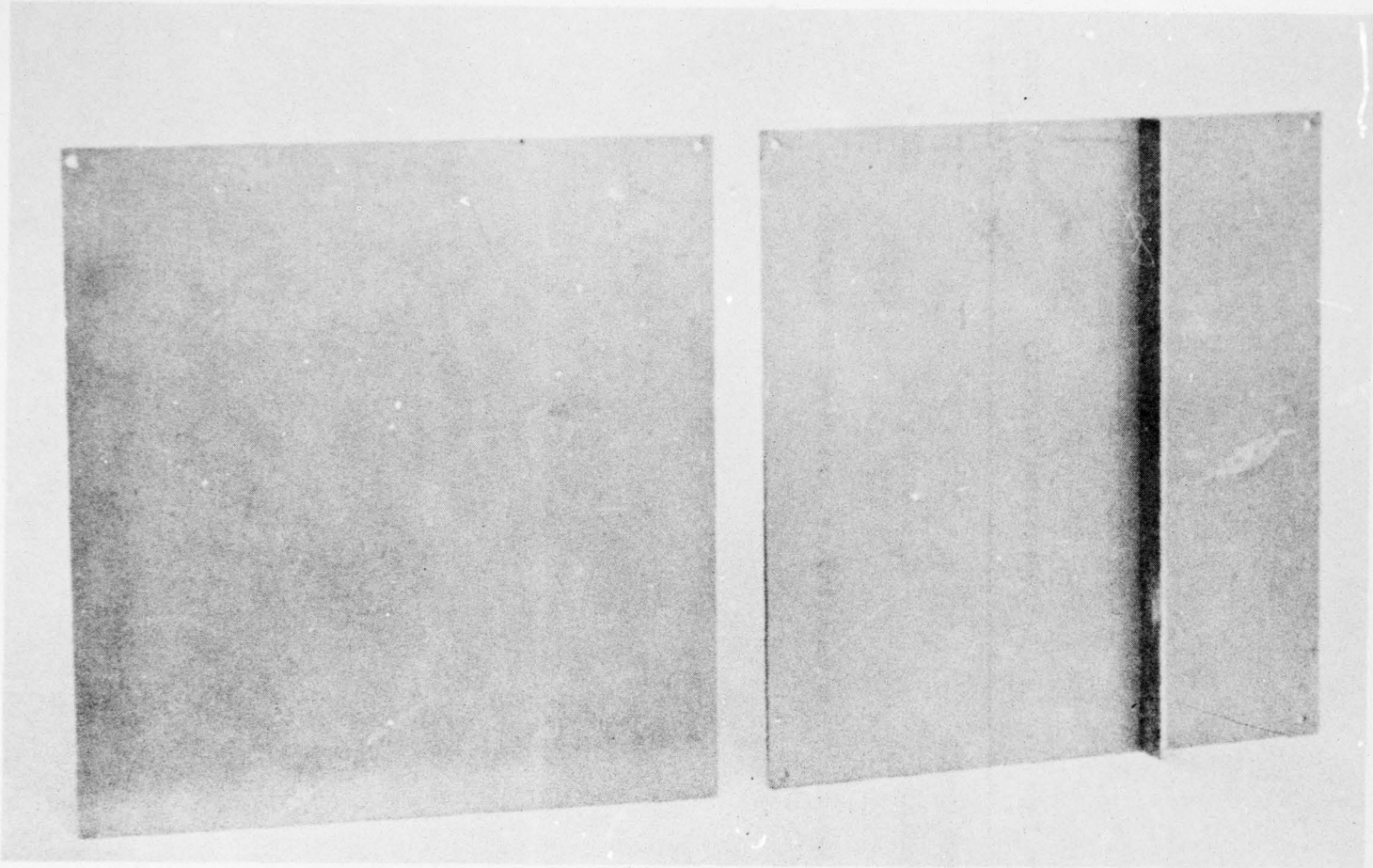

PLAIN PLATE

RIBBED PLATE

FIGURE 1
ACOUSTIC BACKSCATTERING TARGET PLATES

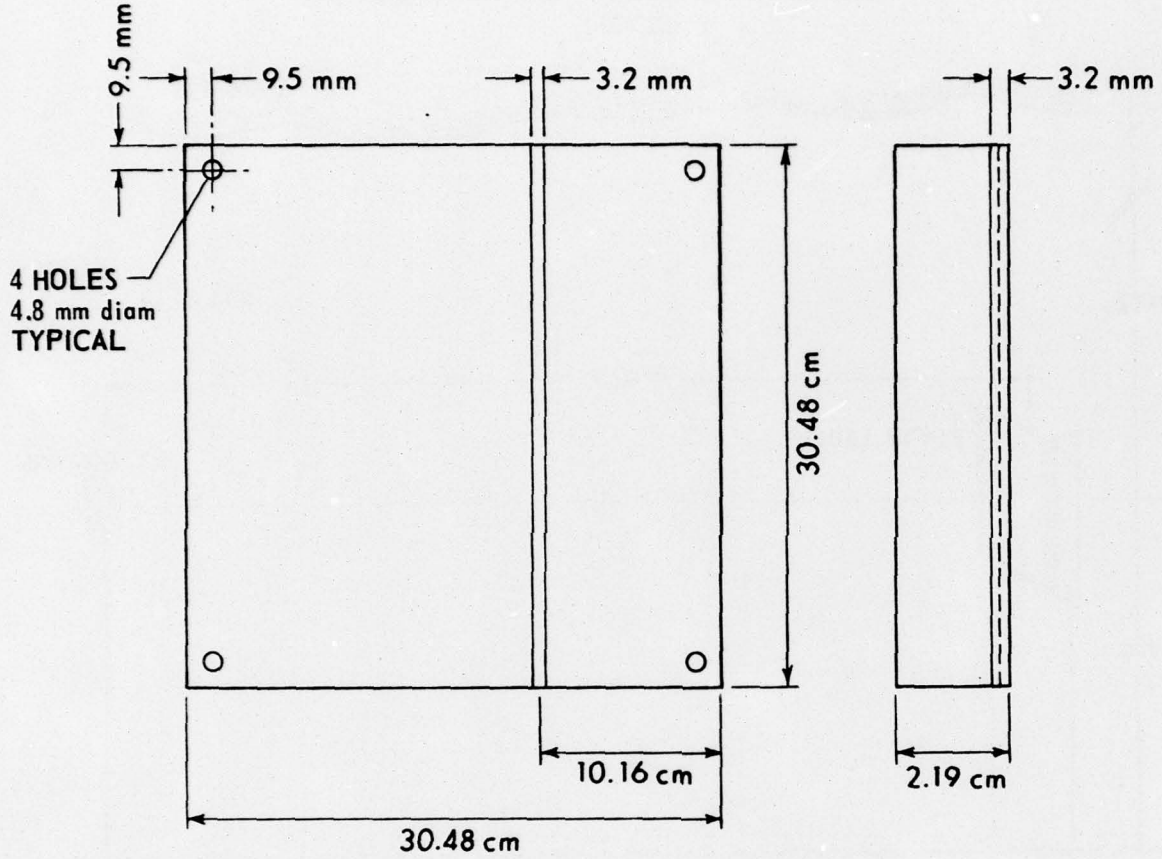

FIGURE 2
ACOUSTIC TARGET PLATE DIMENSIONS

ARL - UT
AS-75-859
KWA - DR
7 - 2 - 75
REV 5-18-77

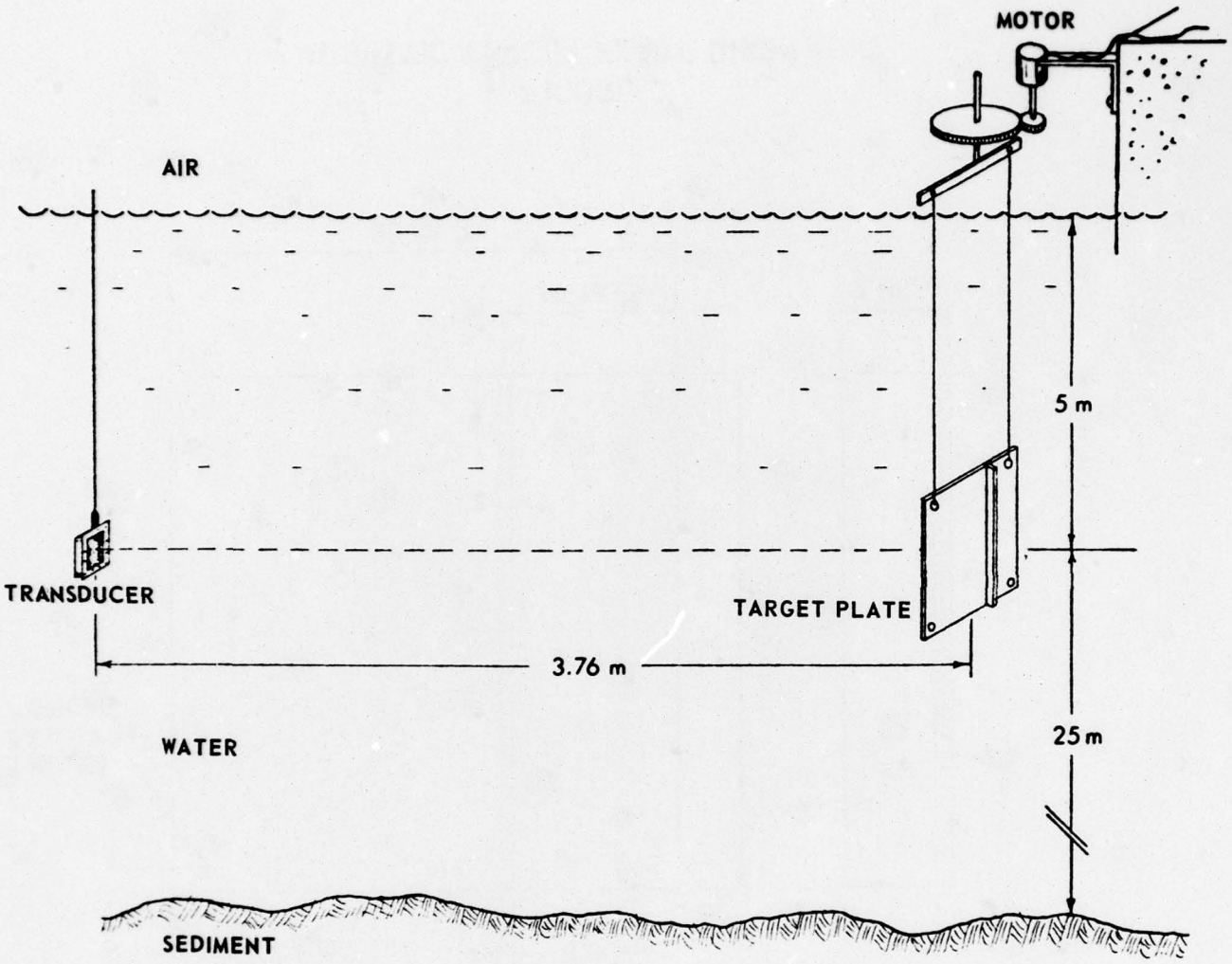

FIGURE 3
GEOMETRIC ARRANGEMENT OF TEST SETUP

ARL - UT
AS-75-860
KWA - DR
5 - 1 - 75
REV 5-31-77

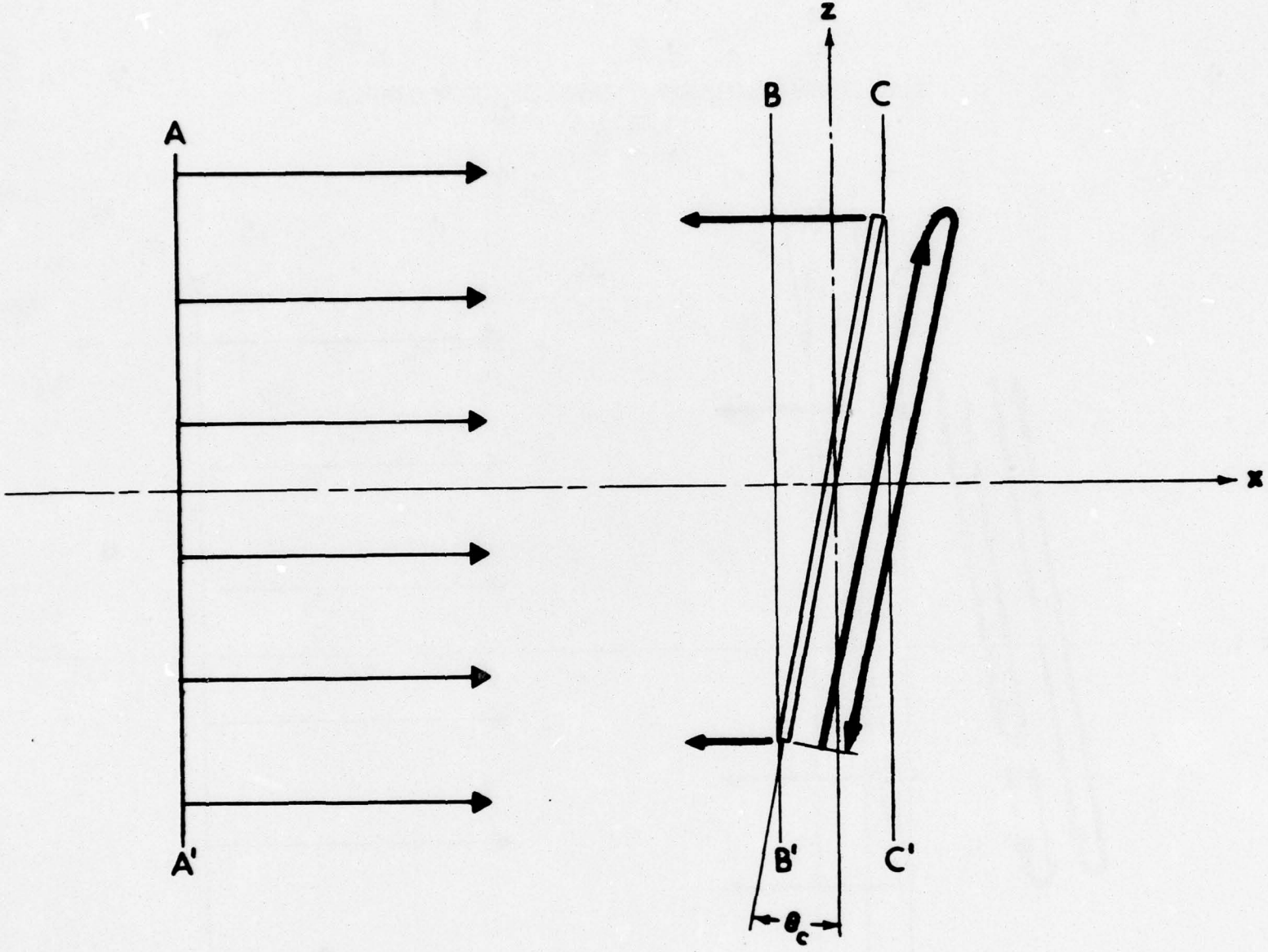

FIGURE 4
ASSUMED ACOUSTIC TRAVEL PATHS FOR PLAIN PLATE

ARL - UT
AS-75-864
KWA - ORS
7 - 3 - 75

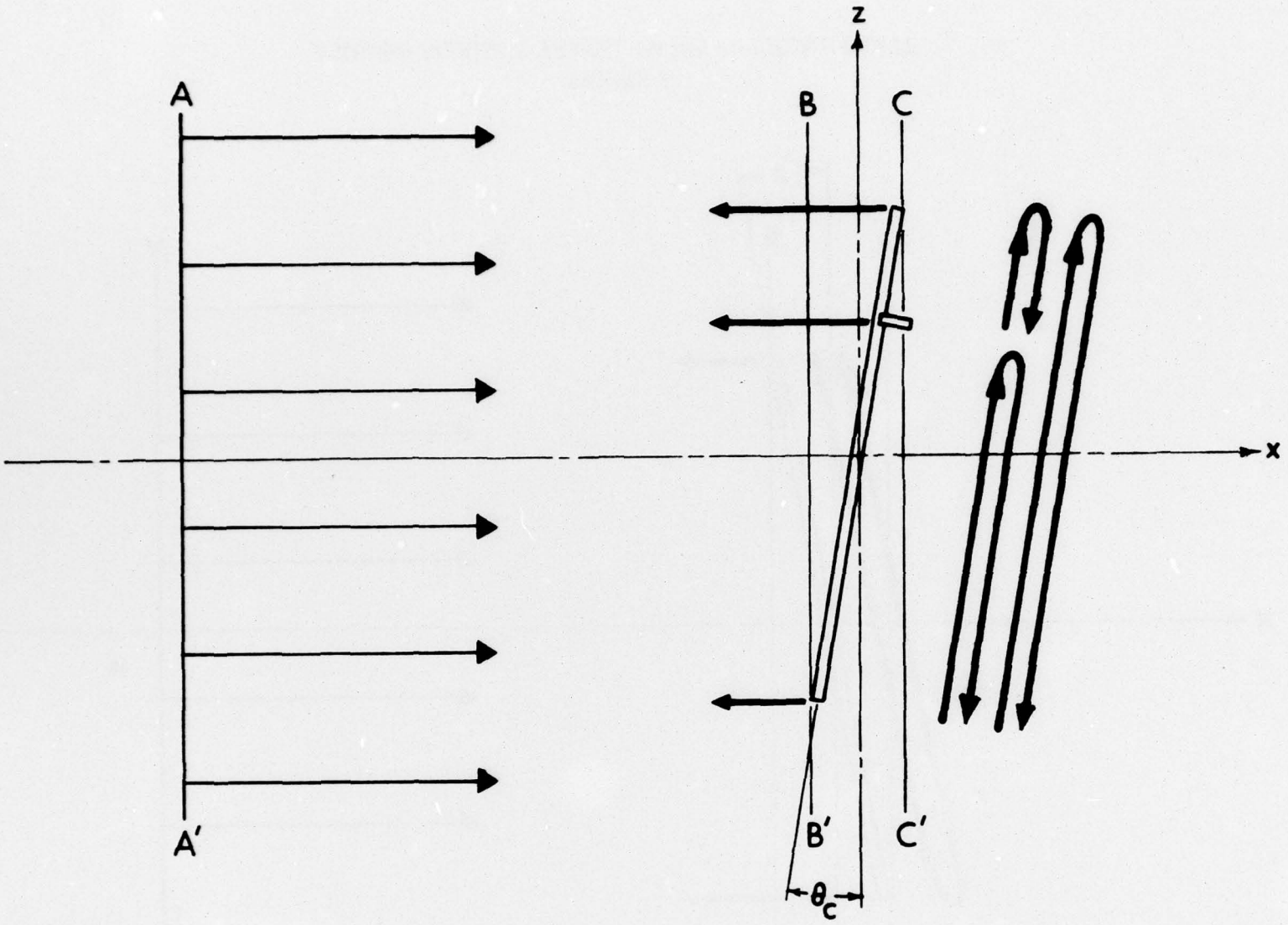

FIGURE 5
ASSUMED ACOUSTIC TRAVEL PATHS FOR RIBBED PLATE

ARL - UT
AS - 75 - 865
KWA - ORS
7 - 3 - 75

angle of incidence, the refracted ray forms an angle of 90° with the normal to the interface at the edge closest to the source, and maximum acoustic energy is coupled into the plate.[23]

The minimum farfield distance measured from the face of the transducer is $R = d_1^2 + d_2^2/\lambda$, where d_1 is the largest dimension of the transducer aperture, d_2 is the plate thickness, and λ is the wavelength.[24] For the transducer shown in Fig. 7 the minimum farfield distance is calculated as

$$R = \frac{10.16^2 + 0.32^2}{2.46} = 42.0 \text{ cm} \quad .$$

Wavelength calculations are given in Appendix A.

If the sound speed in fresh water near the surface is 1484 m/sec at 21°C, and if the longitudinal sound speed in the aluminum plate is 5.45×10^3 m/sec, one obtains a critical angle of target orientation of ±15.79° from the normal to the incident plane wave,[25] as shown in Figs. 4 and 5.

At this water temperature, a one way path time delay of 2.4 msec for the specular echo can be expected, assuming that the target plate is entirely insonified by the 3 dB beamwidth at the test distance of 3.76 m between the face of the transducer and point B' at the nearest corner of the plate. One may next consider the two travel paths within the plain plate, shown in Fig. 4. These paths are formed by the incident sound ray entering the plate at point B' and traveling to point C, where part of the energy is radiated into the water and part of it is reflected back to point B'; then the sequence is repeated. It can be seen from the following calculations that, at the critical angle of incidence, the total travel times for each path are identical.

Path 1: from point B' to C

distance = 30.48 cm

$C_L = 5.45 \times 10^3$ m/sec

→ travel time t_1=55.8 μsec

Path 2: from point C to point B

$\sin \theta_c = \frac{a}{c}$; where distance a = CB
distance c = B'C

$\theta_c = 15.79°$

$0.272 = a/30.48$

a = 8.29 cm

C_{water} = 1484 m/sec

→ travel time t_2 = 55.8 μsec.

Using these identical travel times for both cases, one may expect a pulse after twice this delay, or 111.60 μsec after the specular returns for either a two way path in aluminum or a one way path in aluminum and water. The returns from both paths, however, will arrive at the receiver at the same time and will constructively interfere with each other. Usually, several successive pulses, regularly spaced at 111.60 μsec intervals and decaying logarithmically in amplitude, can be expected to occur under favorable signal-to-noise ratio conditions in the echo structure of the plain plate.

For the stiffened plate, the theoretical echo structure predictions are similar, except that three separate travel paths within the plate are to be considered, as shown in Fig. 5. At the same critical angle θ_c=15.79°, one path traverses the entire length of the plate from point B' to point C, where a part of the energy is coupled into the water and part of it is reflected back to point B', as in the plain plate. A second path originates also at point B' but terminates at the rib, where again part of the energy is transmitted into the water and part of it is reflected back to point B', as for the first path. However, part of this transmitted energy also proceeds within the plate to point C, where once

again some of it is coupled into the water, and the rest is reflected to the rib, as for the other travel paths. This process can be expected to repeat itself several times in all three cases. The calculated travel times for each path are as follows.

Path 1a from point B' to C
distance = 30.48 cm
travel time = 55.8 μsec

1b from point C to B
distance = 8.29 cm
travel time = 55.8 μsec

Path 2 from point B' to the rib
distance = 20.32 cm
travel time = 37.20 μsec

Path 3 from the rib to point C
distance = 10.16 cm
travel time = 18.60 μsec

From these travel time calculations, the echo structure of a stiffened plate can be expected, if the driving frequency is chosen properly, to contain three sets of pulses. All three sets constructively interfere with each other at alternate intervals, and are regularly spaced with 111.60 μsec time delays between them.

Wavelength and sound speed calculations are given in the appendix. The spacing of the individual pulses is given in Tables IV and V, where the arrival times of the pulses from the stiffening rib are given explicitly.

III. EXPERIMENTAL TECHNIQUE

The experimental tests and measurements were conducted at the Lake Travis Test Station (LTTS) facility of Applied Research Laboratories (ARL), The University of Texas at Austin. Figure 1 shows the acoustic backscattering targets used in this study. Two plates 30.48 cm square and 3.2 mm thick were machined from 6061-T6 aluminum alloy. The dimensions and the material of the plates were chosen on the basis of past experience in similar studies. The shape and size of the plates were selected to allow the plate to be both thin and stiff. The aluminum alloy chosen is well known for its ability to support internally guided stress waves. One of the plates was fitted with a stiffening rib; Fig. 2 outlines the physical dimensions and press-fit assembly of the ribbed plate. The stiffener was oriented parallel to one of the edges and was placed asymmetrically on the plate as shown. Structural integrity and simplicity dictated the choice of the material, dimensions, and placement of the stiffening rib; the decisions were also based on the author's experience in related studies at ARL.

By rotating the plate 180° in the vertical plane, the rib could be positioned either on the nearside of the centerline with respect to the transducer or on the farside. The resulting changes in travel times produced discernible changes in echo structure. However, when the same plate was placed in the sound field with the rib oriented horizontally, no changes in echo structure could be discerned that would indicate whether the rib was located in the upper or lower portion of the plate.

Figure 3 shows the geometrical arrangement of the test setup. The targets were suspended in the water by two monofilament nylon lines of 0.8 mm in diameter. They were fastened above the surface of the water to

the 61 cm crossbeam of the remote controlled rotating mechanism. Uniform rotational speeds of about 1.5°/sec are required for accurate adjustment of the angle of incidence. The mean depth of the plates was chosen at 5 m below the surface and about 25 m above the lake bottom. Because of other obstacles and the irregular sloping underwater terrain, this arrangement was considered optimum, and it was possible to avoid interference effects through proper pulse gating techniques. The water path distance between the face of the transducer and the nearest edge of the plate was 3.76 m, resulting in a two way travel time of 5.07 msec at a water temperature of 21°C. To avoid interfering spectral returns, the stiffening rib was positioned in the acoustic shadow of the plate, that is, on the side facing away from the source.

The line AA' in Figs. 4 and 5 represents an assumed plane wavefront approaching the y-z oriented target plates in the positive x direction. The line BB' depicts the time when this incident wave couples into the nearest edge of the plate. If the coupling angle θ is adjusted carefully to its critical value--in this experiment, this value was about 15.8°--the travel times of the sound in the plate from point B' to point C and in the water from point C to point B will be identical, and constructive interference will result in the presentation of a distinct pulse train on the receiving oscilloscope screen.

Figure 6 shows a block diagram of the electronic test equipment used in the experiment. The components are of the laboratory type and were chosen to adequately process the short 30 μsec pulse length and the repetition rate of 30 pulses/sec of the signal frequency. The Hewlett-Packard 651A test oscillator provided a stable, low distortion 60 kHz sine wave signal for the transmit gate of the variable tone burst generator. The Scientific Atlanta pulse timing generator was the clock of the system and provided the proper timing for the receive and transmit cycle of the switching relay. A General Radio model 1206B unit amplifier with unit power supply model 1203B served as the driver for the 50 W

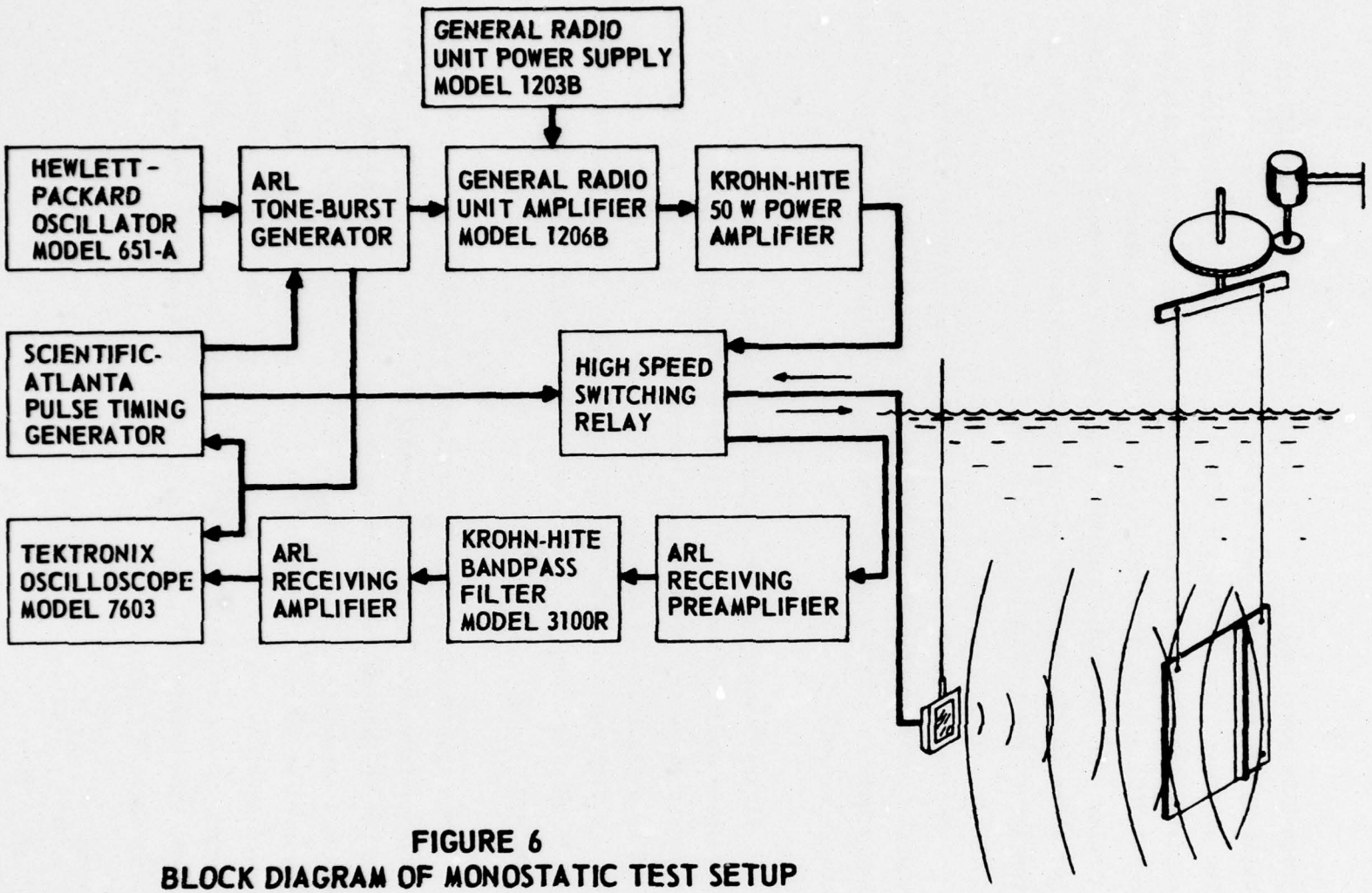

FIGURE 6
BLOCK DIAGRAM OF MONOSTATIC TEST SETUP

ARL - UT
AS-75-866
KWA - DR
7 - 2 - 75
REV 5-18-77

Krohn-Hite power amplifier. The solid state receiving amplifiers were built by ARL and were chosen for their excellent low noise characteristics. The bandpass filters were variable Krohn-Hite model 3100R filters and were adjusted for a passband from 10 to 150 kHz. The Tektronix oscilloscope model 7603 with an attached Polaroid Land camera served as receiver display. An automatic temperature probe and sound velocity recorder, not shown in Fig. 6, recorded a water temperature of 21°C ±0.5°C on the day of the testing.

The monostatic measurement technique was chosen to provide a better signal-to-noise ratio in the received signal. A high speed switching relay made it possible to use the same transducer alternately as source and receiver.

Figure 7 shows the transducer used for this experiment. The effective aperture was a 7.94 x 10.16 cm rectangular array of 15 barium titanate elements. Each element measures 1.90 x 2.54 x 0.64 cm thick and is mass loaded by a 1.90 x 2.54 x 1.59 cm thick steel block cemented to its back surface. The mechanical resonance of this assembly occurs at 73 kHz, as measured by driving the transducer with a step voltage waveform.

The transducer was matched to the power amplifier by means of a resistor-inductor network bypassed during the receive cycle. The values for the resistance and inductance were obtained by tuning the system for maximum bandwidth in the transmit cycle. The signal peak frequency occurred at 60 kHz. The half-power points were 29 and 81 kHz. The source level obtained was +175 dB re 1 μPa at 1 m. The maximum dynamic range without echo distortion was 28 dB. In practice, a range of 25 dB was used. The receiving sensitivity of the transducer was measured to be -210 dB re 1 V/μPa.

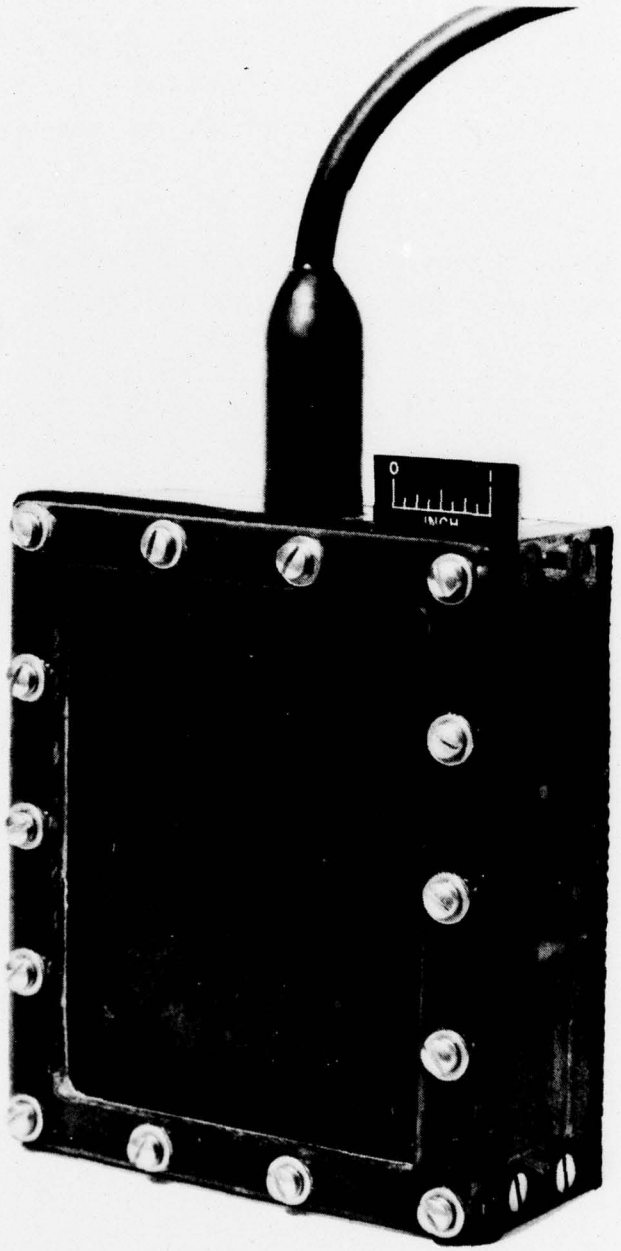

FIGURE 7
TRANSDUCER

Figure 8 shows the horizontal directivity pattern of the transducer with a corresponding -3 dB beamwidth of 13.8°. Figure 9 shows the vertical directivity pattern with a corresponding -3 dB beamwidth of 10.04°. The directivity index[26] for a rectangular aperture and for these beamwidths is 24 dB.

Figure 10 shows the receive sensitivity of the transducer as a function of frequency over the range from 30 to 100 kHz.

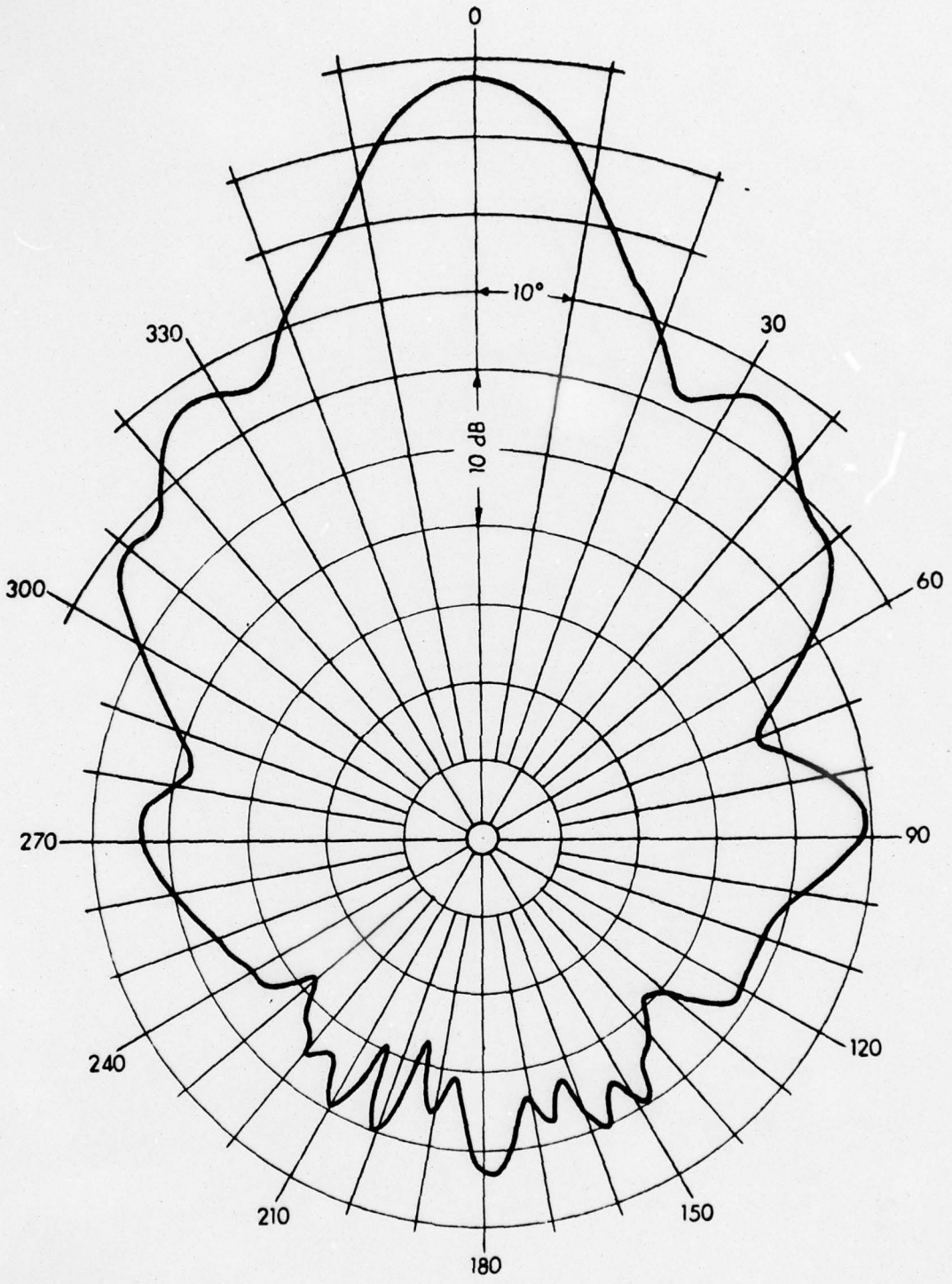

FIGURE 8
HORIZONTAL DIRECTIVITY PATTERN
OF TRANSDUCER

FREQUENCY = 60 kHz

ARL - UT
AS-75-861
KWA - ORS
7 - 2 - 75

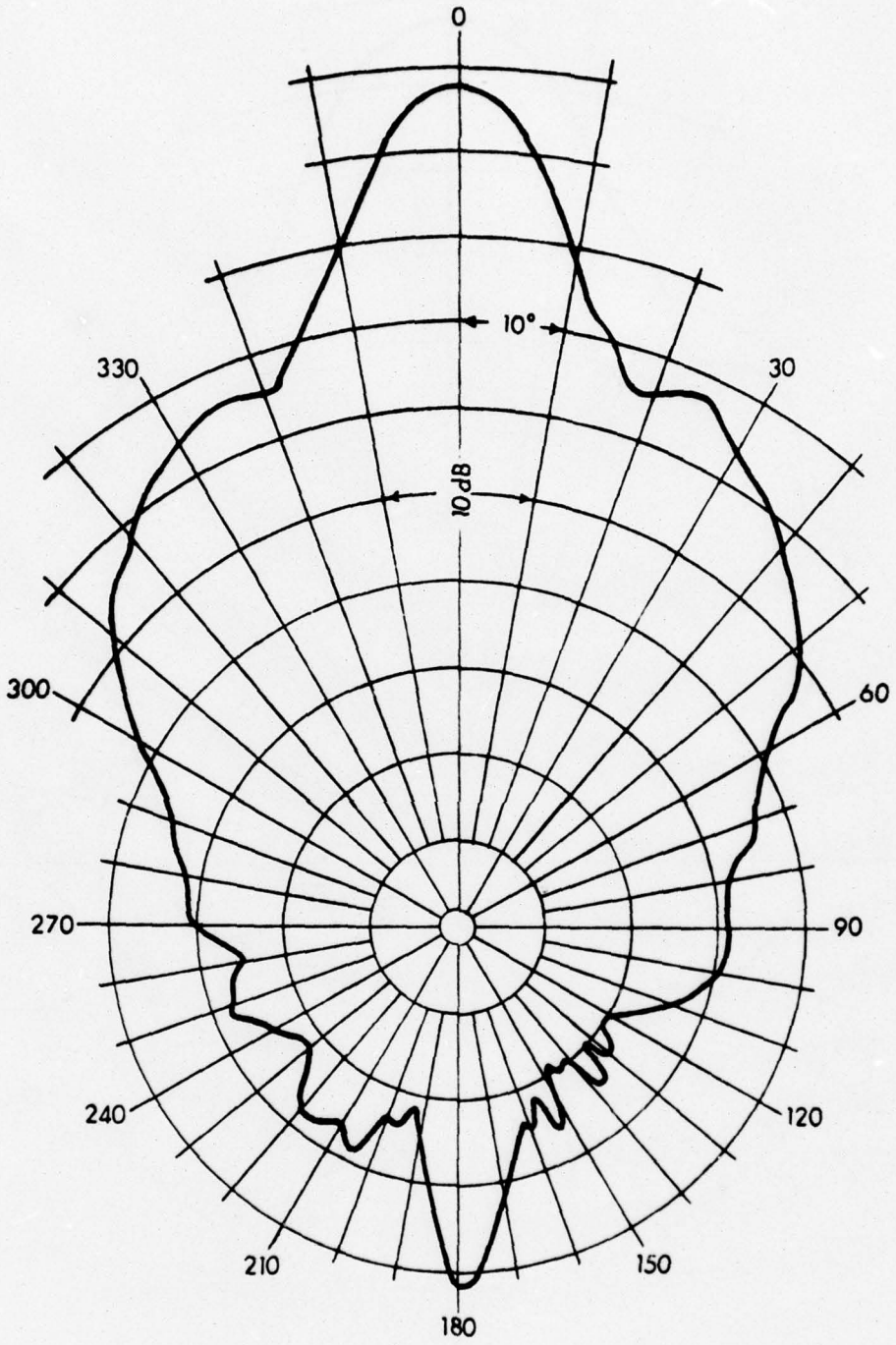

FIGURE 9
VERTICAL DIRECTIVITY PATTERN
OF TRANSDUCER

FREQUENCY = 60 kHz

ARL - UT
AS-75-862
KWA - ORS
7 - 2 - 75

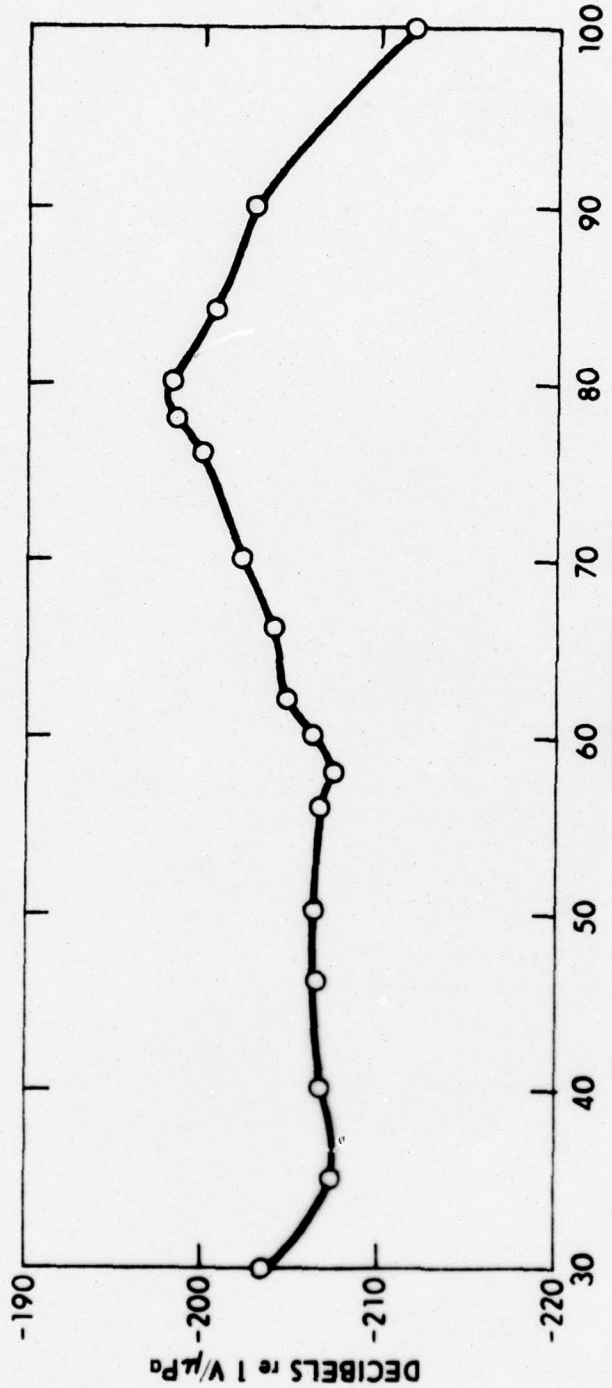

FIGURE 10
RECEIVE SENSITIVITY OF TRANSDUCER

ARL - UT
AS-77-591
KWA - DR
5 - 18 - 77

IV. EXPERIMENTAL RESULTS

The experimental results of this study are shown in Figs. 11 through 14. The echo structure from the plain plate is shown in Fig. 11. Figure 12 shows the return from the horizontally ribbed plate, and Figs. 13 and 14 show the return from the stiffened plate where the rib was placed vertically. Based on these recordings, the travel times of the sound in the plates were measured and compared to the theoretically predicted values presented in section II. The logarithmic decrements associated with the reflections in each travel path shown in Figs. 4 and 5 were determined and tabulated.

After close examination of these recordings and of the calculated propagation speeds of the stress waves mentioned in section II, it was concluded that only longitudinal waves can be discerned. No evidence of other propagation modes was detected under the conditions of this experiment.

A. Travel Times

Close inspection of Fig. 10 reveals that there are two similar sets of pulse trains present. Both sets exhibit the same 112 μsec pulse spacing and decay at approximately the same rate. This pulse train doubling, although it results from a slight misalignment of about 0.1° in the target geometry, is important here, because it illustrates that a pulse is coupled into the water from both ends of the plate. The measured average spacing of 112 μsec is in good agreement with the calculated values for longitudinal waves. Table II compares measured and calculated travel times for the plain plate.

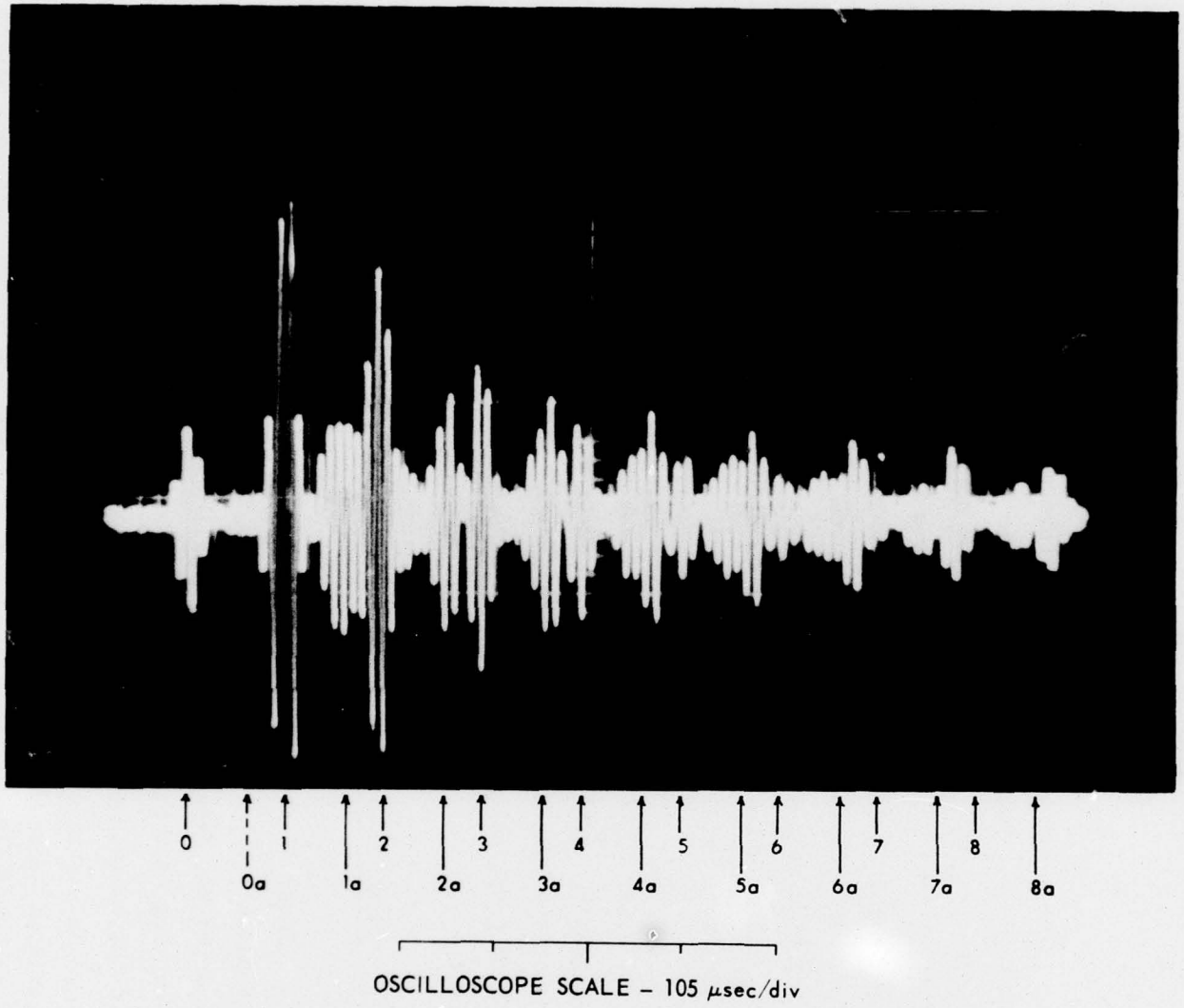

FIGURE 11
ECHO STRUCTURE FROM PLAIN PLATE

ARL - UT
AS-75-901
KWA - RFO
7 - 7 - 75

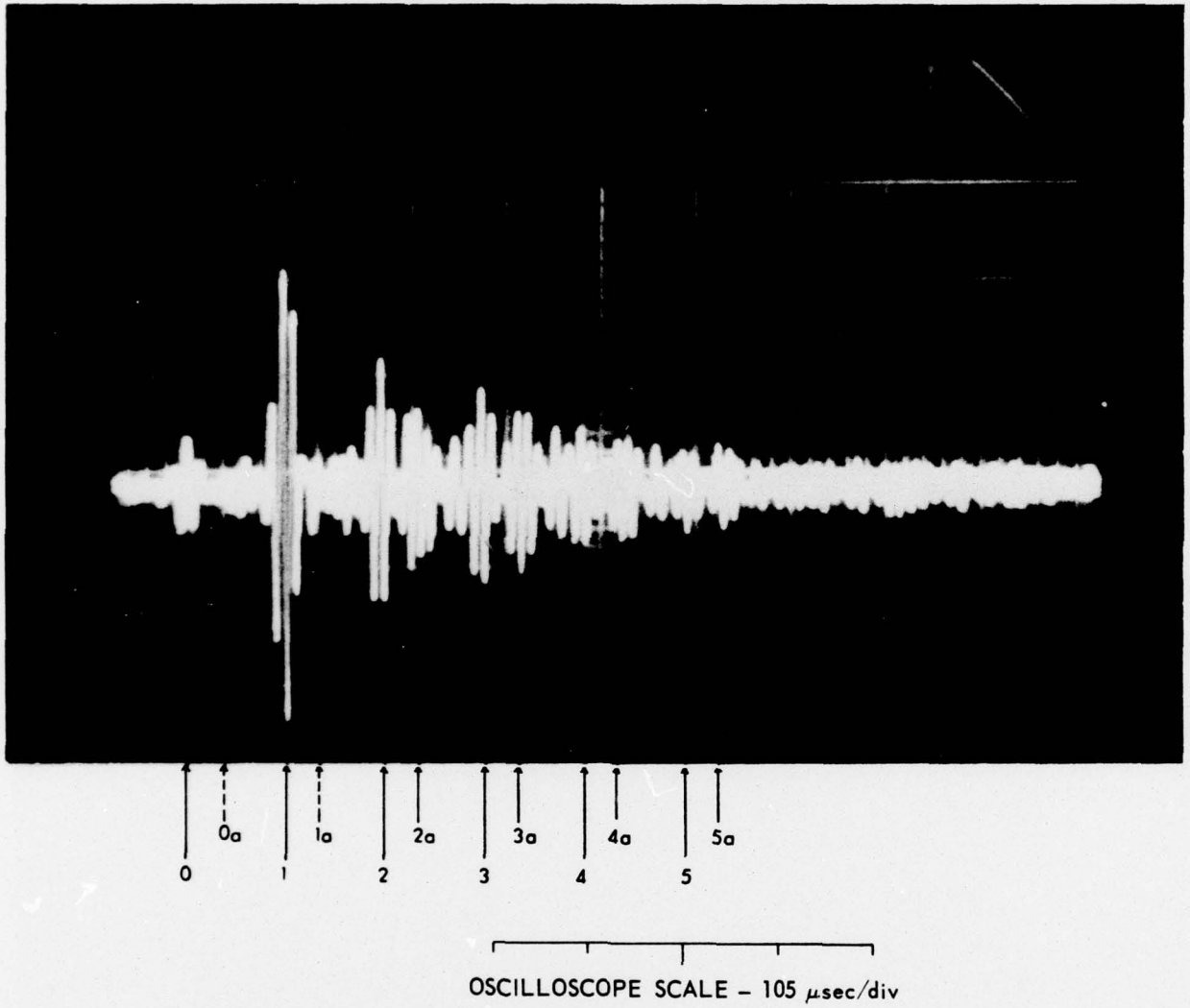

FIGURE 12
ECHO STRUCTURE FROM HORIZONTALLY STIFFENED PLATE

ARL - UT
AS-75-902
KWA - RFO
7 - 7 - 75

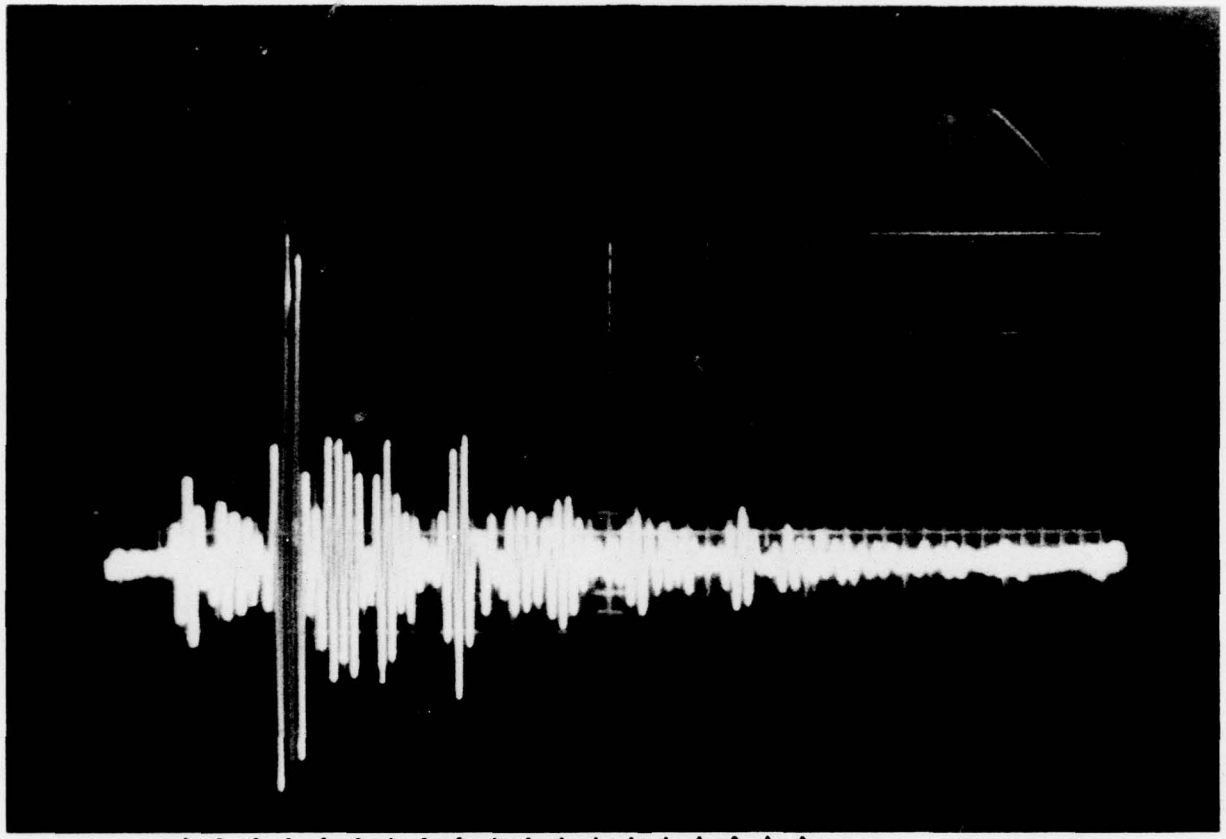

FIGURE 13
ECHO STRUCTURE FROM VERTICALLY STIFFENED PLATE
WITH RIB LOCATED IN NEAR PORTION OF PLATE

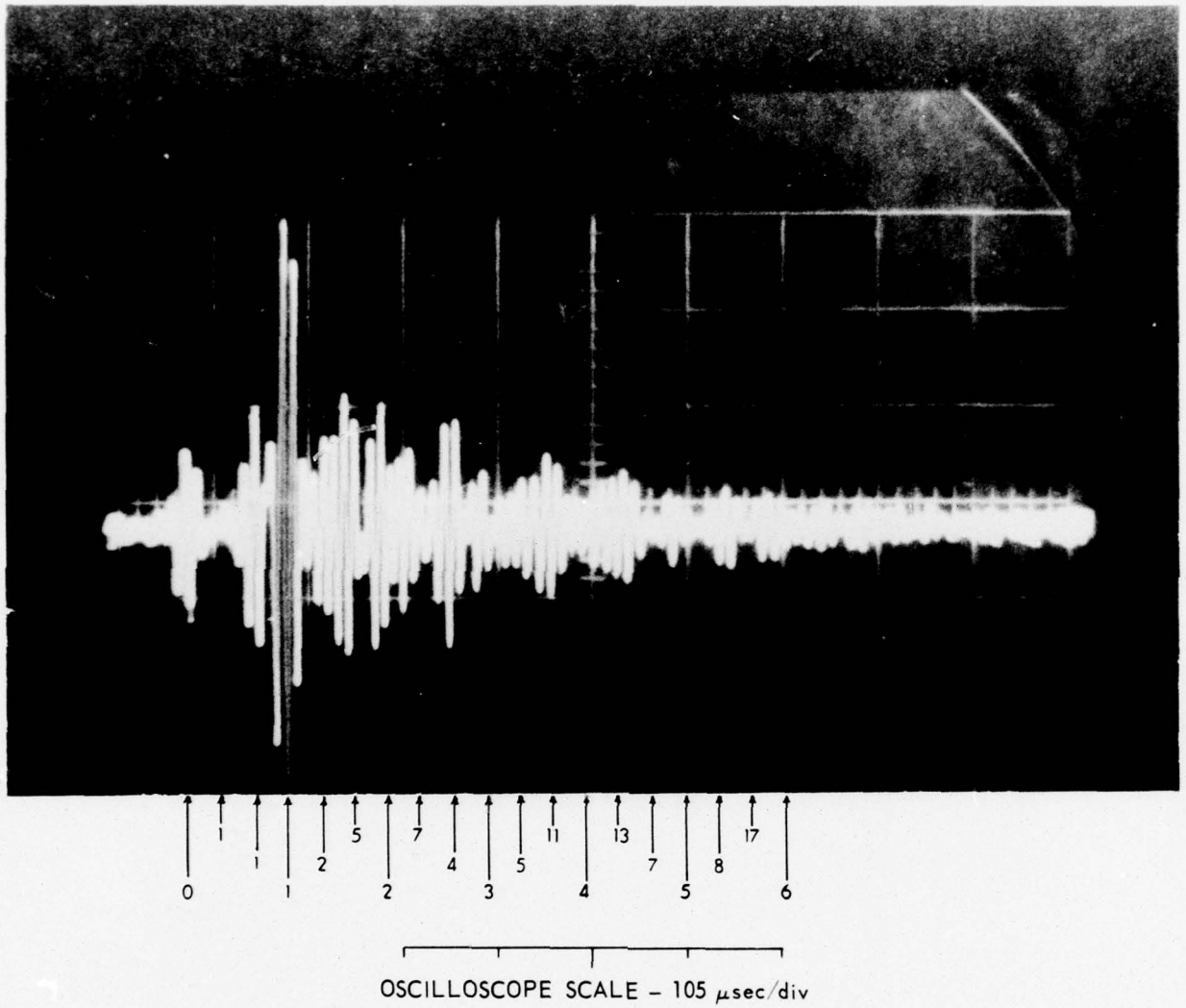

FIGURE 14
ECHO STRUCTURE FROM VERTICALLY STIFFENED PLATE
WITH RIB LOCATED IN FAR PORTION OF THE PLATE

ARL - UT
AS-75-904
KWA - RFO
7 - 7 - 75

TABLE II

PULSES FROM FIGURE 11

Pulse Number	Measured Time μsec	Calculated Time μsec	MT-CT μsec
1	112.4	111.6	+0.8
1a	112.4	111.6	+0.8
2	223.3	223.2	+0.1
2a	225.5	223.2	+2.3
3	336.4	334.8	+1.6
3a	336.4	334.8	+1.6
4	447.4	446.4	+1.0
4a	443.7	446.4	-2.7
5	562.0	558.0	+4.0
5a	565.7	558.0	+7.7
6	672.9	669.6	+3.3
6a	672.9	669.6	+3.3
7	783.8	781.2	+2.6
8	894.7	892.8	+1.9

The standard deviation of the whole set of differences is 2.24 μsec.

The pulse intervals were calculated from the travel times given above. For pulses 1 through 8, the mean pulse interval was 111.8 μsec and the standard deviation was 1.3 μsec; for pulses 1a through 6a, the mean pulse interval was 112.1 μsec and the standard deviation was 4.9 μsec. The much larger standard deviation in the second set was largely caused by the value for pulse 5a, which also gave the largest departure from the calculated value in the measured time minus calculated time (MT-CT) column in the tables.

Figure 12 shows the echo structure from the stiffened plate with the reinforcing rib oriented horizontally. The rib was placed in the acoustic shadow of the plate to avoid geometrical returns. Close inspection of the echo structure reveals that two sets of 111.6 μsec pulse trains are present, similar to the return from the plain plate. Because the angle of incidence was kept the same for both sets of measurements and because the rib does not represent a discontinuity to the longitudinal waves in this direction, this similarity is to be expected. The measured average spacing of 111.6 μsec is in good agreement with the calculated values for longitudinal waves. Table III compares measured and calculated travel times for the horizontally stiffened plate.

The standard deviation of the whole set of differences is 4.44 μsec.

The pulse intervals were calculated from the travel times given above in the Measured Time column. For pulses 1 through 4, the mean pulse interval was 110.9 μsec and the standard deviation was 2.65 μsec. For the set of pulses 2a through 5a, the mean pulse interval was 111.8 μsec and the standard deviation was 6.6 μsec. Whereas the uniformity is not so good as in the earlier set of pulses (Table III), the distribution does not suggest any bias nor the presence of nonrandom errors.

Figures 13 and 14 show the echo structure from the stiffened plate with the rib oriented vertically. The angle of incidence and all electronic

TABLE III

PULSES FROM FIGURE 12

Pulse Number	Measured Time μsec	Calculated Time μsec	MT-CT μsec
1	110.9	111.6	-0.7
2	218.1	223.2	-5.1
2a	218.8	223.2	-4.4
3	329.0	334.8	-5.8
3a	337.0	334.8	+2.2
4	443.7	446.4	-2.7
4a	455.0	446.4	+8.6
5a	558.0	558.0	0

adjustments remained unchanged throughout the entire testing sequence. The pulse train spacings correspond directly to the assumed travel paths shown in Fig. 5. The return from the stiffened plate with the rib located in the near portion of the plate is shown in Fig. 13. The pulse on the far left is the specular echo. The next pulse is the first reflection from the internally guided wave and represents a 37.2 μsec period or 10.16 cm path from the edge to the rib. The second pulse failed to appear after the same spacing and would have been composed of the second 37.2 μsec and the first 74.4 μsec return from the 20.32 cm path between the rib and the far edge. It is believed that destructive interference precluded the detection of the pulse, since the maximum amplitude would have been the sum of the two returns. The third pulse is of large amplitude because it represents the sum of the first 30.48 cm path and the third 10.16 cm path reflection. The fourth pulse shows the second reflection of 20.32 cm path or 74.4 μsec period. The fifth pulse should have appeared 37.2 μsec later but, again because of destructive interference, is not identifiable. The sixth pulse shows the sum of the sixth 37.2 μsec period, the third 74.4 μsec period, and the second 111.6 μsec period. In Table IV the calculated travel times are compared to measured values for the pulses in Fig. 12. The standard deviation of the entire set of differences is 3.47 μsec.

Figure 14 shows the recording from the vertically stiffened plate with the rib located in the far portion of the plate. The recording resembles Fig. 13 except that the first pulse occurs 75.4 μsec after the specular echo and corresponds to an 20.32 cm path from the edge to the rib. The next pulse is the second reflection and is composed of the return from the first 30.48 cm path, or 111.6 μsec, and the first 10.16 cm path, or 37.2 μsec, from the rib to the edge of the plate. The next pulse is considered to be the fourth reflection of the 37.2 μsec pulse, followed by a pulse composed of the third 74.4 μsec path and the second 111.6 μsec path. Following this pattern, these pulses and additional pulses are listed and compared to calculated travel times in

TABLE IV

PULSES FROM FIGURE 13

Pulse Number			Measured Time	Calculated Time	MT-CT
37.2 μsec	74.4 μsec	111.6 μsec	μsec	μsec	μsec
1			36.9	37.2	-0.3
2	1		--	74.4	--
3		1	110.9	111.6	-0.7
4	2		151.6	148.8	+2.8
5			--	186.0	--
6	3	2	218.1	223.2	-5.1
7			--	260.4	--
8	4		299.5	297.6	+1.9
9		3	329.0	334.8	-5.8
10	5		366.0	372.0	-6.0
11			410.4	409.2	+1.2
12	6	4	--	446.4	--
13			484.3	483.6	+0.7
14	7		--	520.8	--
15		5	--	558.0	--
16	8		598.9	592.2	+6.7
17			--	632.4	--
18	9	6	667.7	669.6	-1.9

Table V. The omission of measured travel times indicates that no reliable measurement could be obtained.

The standard deviation of the whole set of differences is 4.21 μsec.

Not all pulses in these recordings have been identified; however, since the angle of incidence remained unchanged, it appears that some of the unidentifiable returns are caused by the pulse doubling mentioned earlier. No attempt was made to hypothesize values for the unobtainable readings. The analysis is based entirely on the values measured. The good agreement and lack of bias show that the theory correctly predicts the experimental results. The interval $[\bar{M}-\sigma, \bar{M}+\sigma]$ is about 8 μsec wide for all four distributions. This spread corresponds to about half of the period of the carrier frequency. It is felt that such a close agreement between theory and practice fully substantiates the theory developed in section II.

B. Logarithmic Decrement

Decay rates for the pulse trains shown in Figs. 11 through 14 were calculated in the form of logarithmic decrements to compare the reflection characteristics of the plate edges to the reflection characteristics of the stiffening rib. The 37.2 μsec and 74.4 μsec periods that correspond to the 10.16 cm and 20.32 cm paths, respectively, between the rib and the plate could not be reliably identified separately; consequently, the logarithmic decrement shown represents the sum of the two periods. The pulse amplitudes used in these calculations are peak to peak values measured in centimeters directly on the enlarged photographs in Figs. 11 through 14. Since the logarithmic decrement is a dimensionless ratio, correcting these readings by the appropriate scale factors was unnecessary. The abscissa shows the number of times that the pulse has been reflected at the edges of the plate or at the rib. The values for the slopes were determined by the method of least squares for variation in a single variable.

TABLE V

PULSES FROM FIGURE 14

Pulse Number			Measured Time	Calculated Time	MT-CT
37.2 μsec	74.4 μsec	111.6 μsec	μsec	μsec	μsec
1			--	--	--
2	1		75.4	74.4	+1.0
3		1	110.9	111.6	-0.7
4	2		--	148.8	--
5			181.2	186.0	-4.8
6	3	2	218.1	223.2	-5.1
7			255.1	260.4	-5.3
8	4		295.8	297.6	-1.8
9		3	336.4	334.8	+1.6
10	5		--	372.0	--
11			406.6	409.2	-2.6
12	6	4	--	446.4	--
13			448.0	483.6	+5.0
14	7		--	520.8	--
15		5	550.0	558.0	-8.0
16	8		602.6	595.2	+6.6
17			--	632.4	--
18	9	6	665.5	669.6	-4.1

The logarithmic decrements δ for the plain and stiffened plates are shown graphically in Figs. 15 through 18 and are calculated numerically as follows.

1. Plain plate

x_{4a} = peak-to-peak amplitude of 4th pulse = 2.08 cm

x_{5a} = peak-to-peak amplitude of 5th pulse = 1.34 cm

$$\delta = \ln\left(\frac{x_{4a}}{x_{5a}}\right)$$

$$= \ln\left(\frac{2.08}{1.34}\right)$$

$$= 0.44$$

2. Ribbed plate with rib mounted horizontally

x_1 = peak-to-peak amplitude of 1st pulse = 6.50 cm

x_3 = peak-to-peak amplitude of 3rd pulse = 2.65 cm

$$2\delta = \ln\left(\frac{x_1}{x_3}\right)$$

$$\delta = 1/2 \left[\ln\left(\frac{6.50}{2.65}\right)\right]$$

$$= 0.45$$

3. Ribbed plate with rib mounted vertically in near portion of the plate

a. logarithmic decrement δ_E for pulses reflected from the edges

x_1 = peak-to-peak amplitude of 1st pulse = 9.35 cm

x_2 = peak-to-peak amplitude of 2nd pulse = 3.60 cm

$$\delta = \ln\left(\frac{x_1}{x_2}\right)$$

$$\delta_E = \ln\left(\frac{9.35}{3.60}\right)$$

$$= 0.95$$

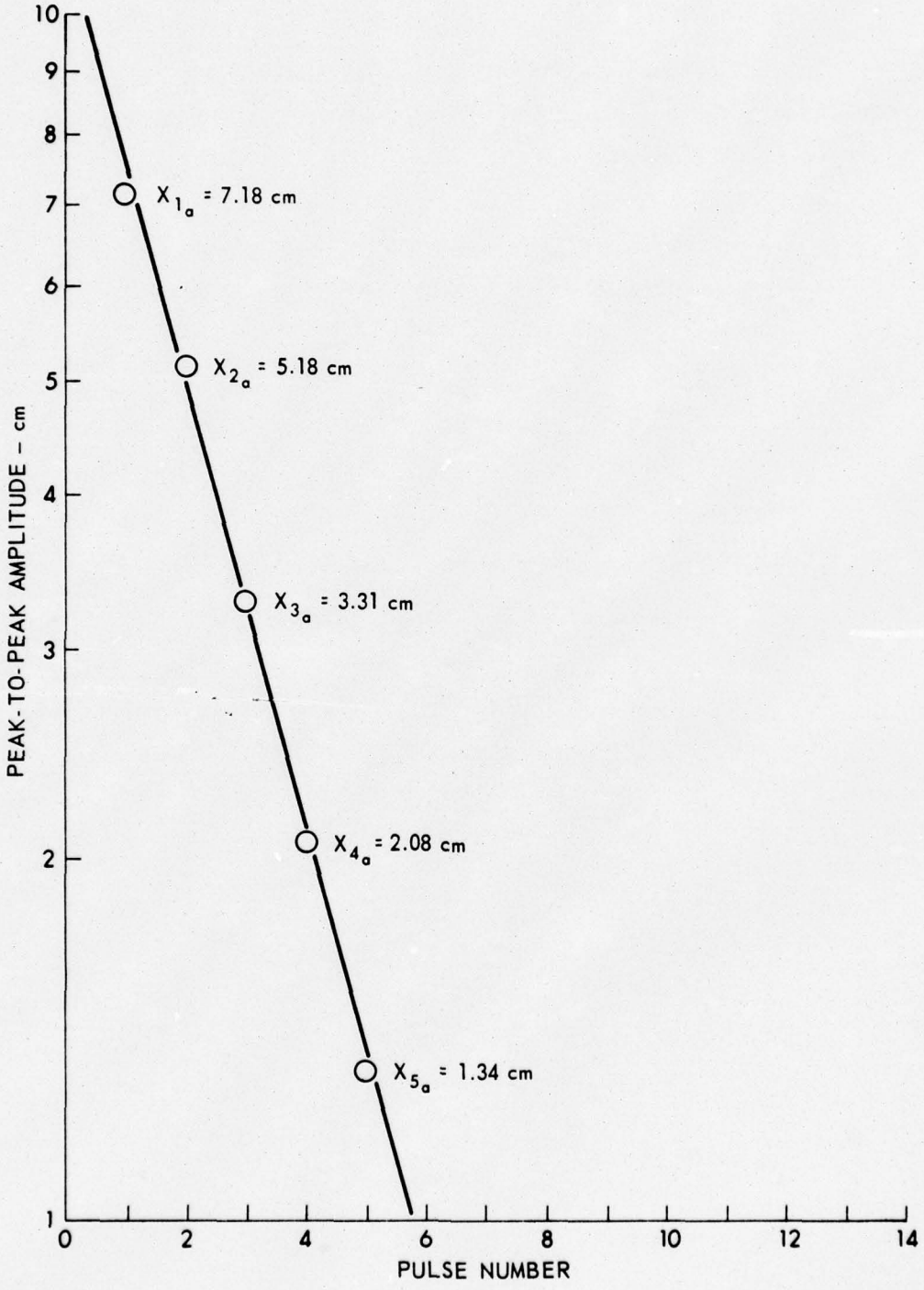

FIGURE 15
LOGARITHMIC DECREMENT OF PLAIN PLATE

ARL - UT
AS-75-868
KWA - DR
7 - 3 - 75

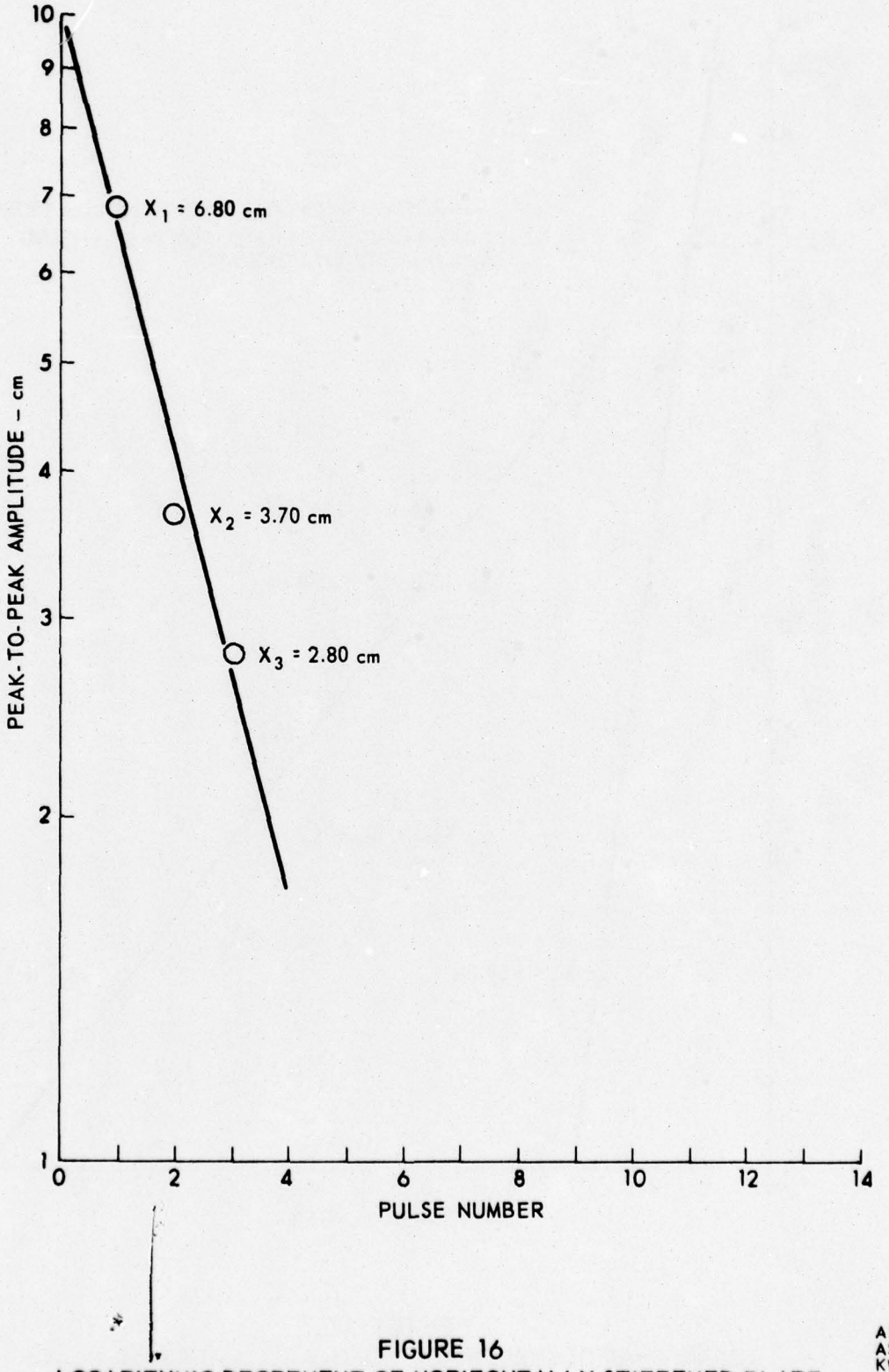

FIGURE 16
LOGARITHMIC DECREMENT OF HORIZONTALLY STIFFENED PLATE

ARL - UT
AS-75-869
KWA - DR
7 - 3 - 75

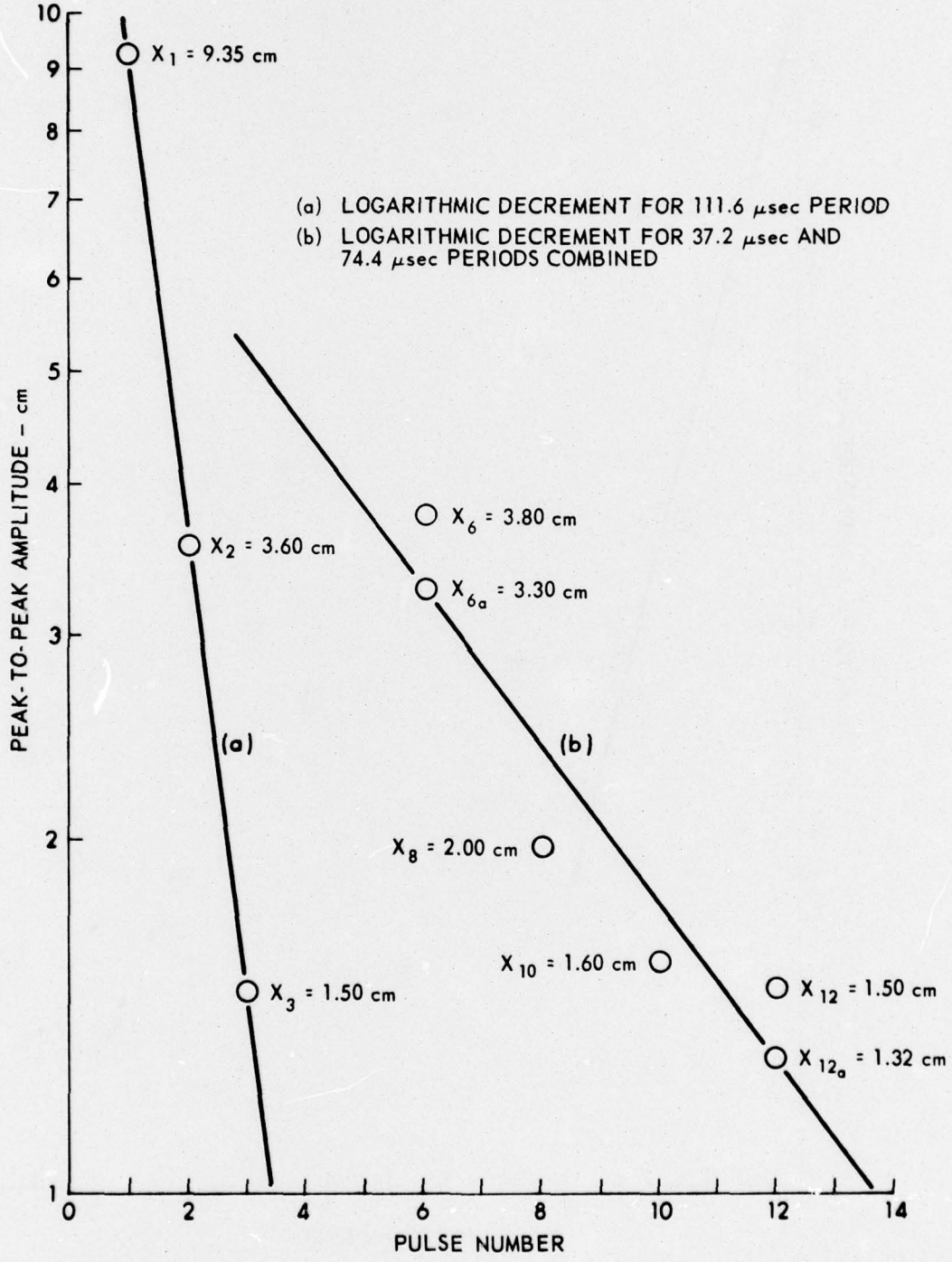

FIGURE 17
LOGARITHMIC DECREMENT OF VERTICALLY STIFFENED PLATE WITH THE RIB LOCATED IN NEAR PORTION OF THE PLATE

ARL - UT
AS-75-870
KWA - DR
7 - 3 - 75

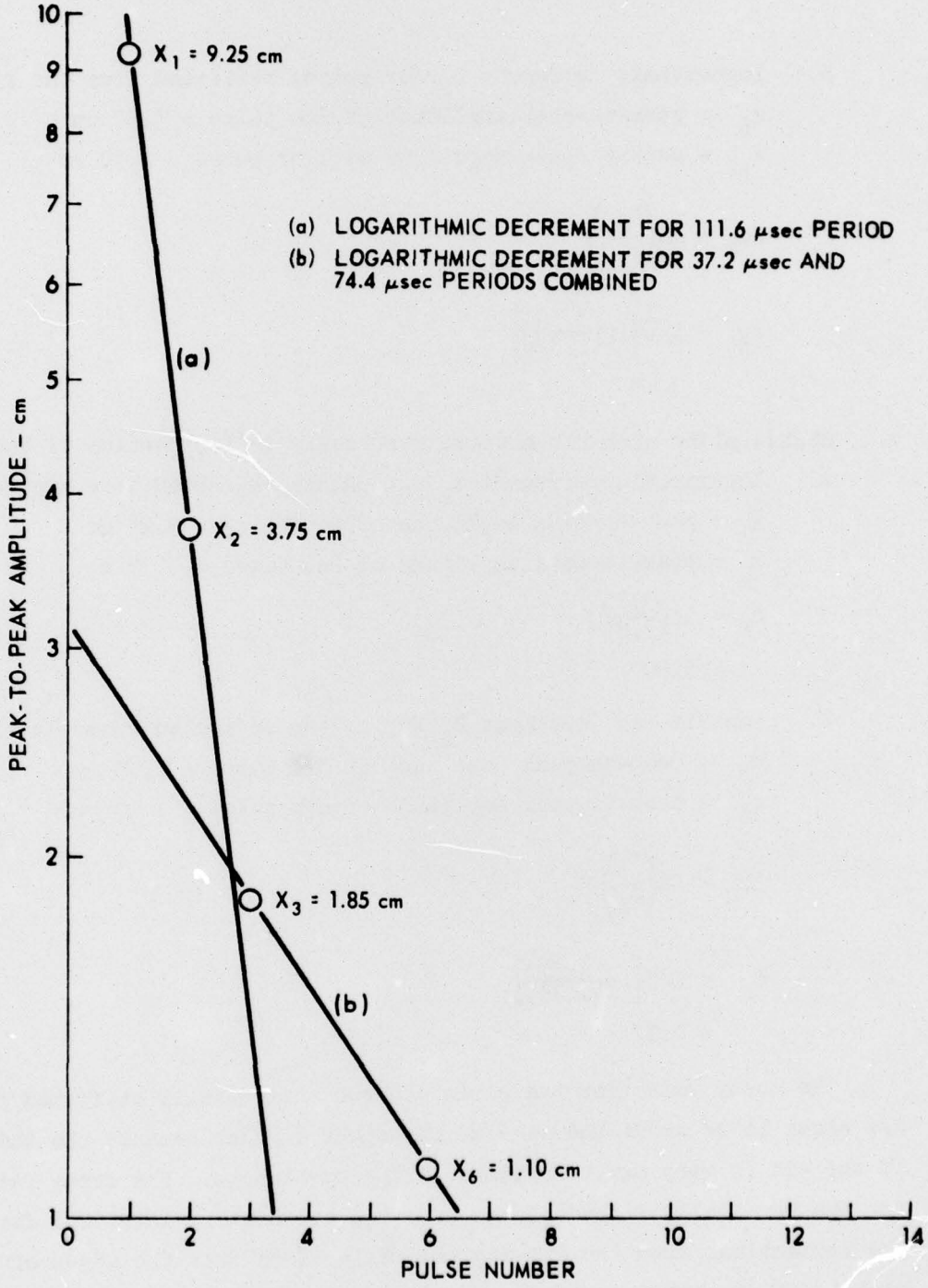

FIGURE 18
LOGARITHMIC DECREMENT OF VERTICALLY STIFFENED PLATE WITH THE RIB LOCATED IN THE FAR PORTION OF THE PLATE

ARL - UT
AS-75-871
KWA - DR
7 - 3 - 75

b. logarithmic decrement δ_R for pulses reflected from the rib

x_6 = peak-to-peak amplitude of 6th pulse = 3.30 cm

x_{12} = peak-to-peak amplitude of 12th pulse = 1.32 cm

$$6\delta_R = \ln\left(\frac{x_6}{x_{12}}\right)$$

$$\delta_R = 1/6\left[\ln\left(\frac{3.30}{1.32}\right)\right]$$

$$= 0.15$$

4. Ribbed plate with rib mounted vertically in far portion of the plate

a. logarithmic decrement δ_E for pulses reflected from the edges

x_1 = peak-to-peak amplitude of 1st pulse = 9.25 cm

x_2 = peak-to-peak amplitude of 2nd pulse = 3.75 cm

$$\delta_E = \ln\left(\frac{9.25}{3.75}\right)$$

$$= 0.90$$

b. logarithmic decrement δ_R for pulses reflected from the rib

x_3 = peak-to-peak amplitude of 3rd pulse = 1.85 cm

x_6 = peak-to-peak amplitude of 6th pulse = 1.10 cm

$$3\delta_R = \ln\left(\frac{x_3}{x_6}\right)$$

$$\delta_R = 1/3\left[\ln\left(\frac{1.85}{1.10}\right)\right]$$

$$= 0.17$$

The decay rates for the plain and the horizontally stiffened plates are shown to be about the same as one might expect, because the thickness of the rib is very small compared to the wavelength. The decay rates for the vertically ribbed plates are also essentially identical for both the reflections from the rib and the reflections from the edges of the plate. Of special importance, however, is the fact that, for both rib locations on the vertically stiffened plate, the amplitudes of the rib reflections seem to diminish about six times more slowly than the amplitudes of the reflections from the plate edges. An explanation of this

result may perhaps be found in the difference between the acoustic impedances encountered at the rib and at the edge.

It is also of interest to note that the decay rate of the horizontally stiffened plate, which is similar to the plain plate, increases significantly when the plate is rotated 90° to the configuration of the vertically stiffened plate. Whether the rib was in the near or far position with respect to the source, the logarithmic decrements of the 30.48 cm periods were doubled, indicating that the pulse amplitudes will decay about twice as fast in the ribbed configuration as they do in the plain or uniform plate.

V. SUMMARY AND CONCLUSIONS

This report has presented evidence of the presence of internally guided longitudinal stress waves in a finite thin aluminum plate with a discontinuity in the form of an attached stiffening rib. With the assumption that the internally guided stress waves are reflected at the discontinuity, it was possible to calculate theoretical travel times and pulse reflection periods. Calculated travel times and critical angle of incidence were confirmed by good agreement with experimentally obtained values, which revealed the presence and fixed the location of the reinforcing rib.

This report has also presented evidence that pulse decay rates in the form of logarithmic decrements of internally guided longitudinal stress waves are a significant clue to the presence and location of reinforcing ribs in thin plates. The logarithmic decrement for a stiffened plate is much higher than for a plain plate. The decay rates of pulse periods corresponding to the reflections from the stiffening rib are shown to be much lower than the pulse periods associated with the reflections from the edge of the plate.

APPENDIX A

WAVELENGTH AND WAVELENGTH-TO-THICKNESS RATIO CALCULATIONS

c = longitudinal sound velocity

f = carrier frequency

λ = wavelength

plate:

$$\lambda = \frac{c}{f} = \frac{1.79 \times 10^4}{6.000 \times 10^4} = 0.298 \text{ ft} = 3.58 \text{ in.}$$

$$= 9.1 \text{ cm}$$

water:

$$\lambda = \frac{c}{f} = \frac{4.87 \times 10^3}{6.000 \times 10^4} = 0.0812 \text{ ft} = 0.97 \text{ in.}$$

$$= 2.5 \text{ cm}$$

plate:

d = 3.2 mm

λ = 91 mm

$$\frac{d}{\lambda} = \frac{3.2}{91} = 0.035$$

APPENDIX B

SOUND SPEED CALCULATIONS IN PLATE

For 6061-T6 aluminum alloy, one obtains

weight density, $\rho_w = 168.5$ lb/ft^3 = 0.0975 lb/in.^{3};

Young's modulus of elasticity, $E = 1.0 \times 10^7$ lb/in.^{2}; and

Poisson's ratio $\nu = 0.3$.

Since E and ν are only known to one significant figure, the implied range of values is

$$0.25 \leq \nu \leq 0.35$$

$$9.5 \times 10^6 \text{ lb/in.}^2 \leq E \leq 10.5 \times 10^6 \text{ lb/in.}^2 \quad .$$

The sound velocity in the aluminum plate was determined experimentally to be 1.79×10^4 ft/sec.

For the relation $C_L = \sqrt{\frac{E}{\rho_m}} \quad \sqrt{\frac{1}{1 - \nu^2}}$

or
$$\frac{C_L}{\sqrt{\frac{1}{1 - \nu^2}}} = \sqrt{\frac{E}{\rho_m}} \quad , \tag{1}$$

we have for $\nu = 0.3$, $\sqrt{\frac{1}{1 - \nu^2}} = 1.05$

and $C_L = 1.79 \times 10^4 \times 12$ in./sec $= 2.148 \times 10^5$ in./sec $= 5.45 \times 10^3$ m/sec .

Now $\rho_m = \frac{\rho_w}{g} \frac{\text{lb/in.}^3}{\text{ft/sec}^2}$ or $\frac{\rho_w}{12g} \frac{\text{lb/sec}^2}{\text{in.}^4}$,

whence $\rho_m = \frac{0.0975}{386.4} \frac{\text{lb/sec}^2}{\text{in.}^4}$

$$= 2.52 \times 10^{-4} \frac{\text{lb/sec}^2}{\text{in.}^4}$$

Thus (1) becomes

$$\frac{2.148 \times 10^5}{1.05} = \sqrt{\frac{E}{2.52 \times 10^{-4}}} \quad ,$$

whence $$\sqrt{E} = \frac{2.148 \times 10^5 \sqrt{2.52 \times 10^{-4}}}{1.05}$$

$$= \frac{2.148 \times 10^5 \times 1.587 \times 10^{-2}}{1.05}$$

$$= \frac{3.41 \times 10^3}{1.05} = 3.25 \times 10^3$$

and $$E = 1.06 \times 10^7 \text{ lb/in.}^2$$

$$= 7.31 \times 10^{10} \text{ N/m}^2$$

$$C_{Bar} = \sqrt{\frac{E}{\rho_m}} = \sqrt{\frac{1.06 \times 10^7}{2.52 \times 10^{-4}}}$$

$$= \sqrt{4.206 \times 10^{10}}$$

$$= 2.05 \times 10^5 \text{ in./sec}$$

$$= 1.71 \times 10^4 \text{ ft/sec}$$

$$= 5.21 \times 10^3 \text{ m/sec}$$

$$C_L = \sqrt{\frac{E}{\rho_m}} \sqrt{\frac{1}{1 - \sigma^2}}$$

$$= 1.71 \times 10^4 \times 1.05$$

$$= 1.79 \times 10^4 \text{ ft/sec}$$

$$= 5.45 \times 10^3 \text{ m/sec}$$

$$C_F = \left(\sqrt[4]{\frac{E}{\rho_m}} \sqrt[4]{\frac{1}{1 - \sigma^2}} \right) \sqrt[4]{\kappa^2} \sqrt{\omega}$$

$$= \sqrt{C_L} \sqrt{\kappa} \sqrt{\omega} \quad .$$

Now $a = \frac{1}{8}$ in. $= \frac{1}{8 \times 12}$ ft $= 1.042 \times 10^{-2}$ ft

$$\kappa = \frac{a}{\sqrt{12}} = \frac{1.042 \times 10^{-2}}{3.464} = 3.01 \times 10^{-3}$$

$$\kappa^2 = 9.06 \times 10^{-6}$$

and $\omega = 2\pi f = 2 \times 3.142 \times 6.000 \times 10^4$

$$= 3.770 \times 10^5 \text{ rad/sec}$$

$$\sqrt{\omega} = 6.14 \times 10^2 \text{ (rad/sec)}^{1/2} \quad .$$

Thus $$C_F = \sqrt[4]{\frac{E}{\rho_m}} \quad \sqrt[4]{\frac{1}{1 - \sigma^2}} \quad \sqrt[4]{\kappa^2} \quad \sqrt{\omega}$$

$$= \sqrt{C_L} \quad \sqrt{\kappa} \quad \sqrt{\omega}$$

$$= \sqrt{1.79 \times 10^4} \quad \sqrt{3.01 \times 10^{-3}} \quad (6.14 \times 10^2)$$

$$= \sqrt{5.388 \times 10} \quad (6.14 \times 10^2)$$

$$= \sqrt{53.88} \quad (6.14 \times 10^2)$$

$$= 7.34 \times 6.14 \times 10^2$$

$$= 4.51 \times 10^3 \text{ ft/sec}$$

$$= 1.37 \times 10^3 \text{ m/sec} \quad .$$

ACKNOWLEDGEMENTS

The author wishes to thank Dr. C. W. Horton, Sr., Dr. C. M. McKinney, Mr. R. H. Wallace, and Mr. K. J. Diercks for their advice and assistance in the preparation of this report. Mr. R. M. Adams deserves special thanks for his many helpful criticisms and suggestions.

REFERENCES

1. C. W. Horton, Sr., J. Acoust. Soc. Am. 51, 1049 (1972).

2. Lord Rayleigh, Theory of Sound (Dover Publications, New York, 1945).

3. P. M. Morse, Vibration and Sound (McGraw-Hill Book Company, Inc., New York, 1936).

4. J. J. Faran, Jr., J. Acoust. Soc. Am. 23, 405 (1951).

5. J. J. Bowman, T. B. A. Senior, and P. L. E. Uslenghi, Electro-Magnetic and Acoustic Scattering by Simple Shapes (North-Holland Publishing Company, Amsterdam; John Wiley and Sons, Inc., New York, 1969).

6. W. Franz and K. Deppermann, Ann. Physik. 10, 361 (1952).

7. K. J. Diercks, T. G. Goldsberry, and C. W. Horton, Sr., J. Acoust. Soc. Am. 35, 59 (1963).

8. G. R. Barnard and C. M. McKinney, J. Acoust. Soc. Am. 33, 266 (1961).

9. K. J. Diercks and T. G. Goldsberry, J. Acoust. Soc. Am 35(A), (1963).

10. C. W. Horton, Sr., W. R. King, and K. J. Diercks, J. Acoust. Soc. Am. 34, 1929 (1962).

11. T. G. Goldsberry, J. Acoust. Soc. Am. 42, 1298 (1967).

12. T. F. Hueter and R. H. Bolt, Sonics (John Wiley and Sons, Inc., New York, 1955) p. 28.

13. K. J. Diercks, K. McCormack, and D. B. James, J. Acoust. Soc. Am. 34, 1957 (1962). See also appendix of this report for wavelength calculations.

14. T. F. Hueter and R. H. Bolt, op. cit., p. 27.

15. Alexander Wood, Acoustics (Dover Publications, Inc., 1966), p. 74.

16. T. F. Hueter and R. H. Bolt, op. cit., p. 28.

17. R. J. Roark, Formulas for Stress and Strain (McGraw-Hill Book Company, Inc., New York, 1965), p. 416.

18. C. D. Hodgeman, ed., Handbook of Chemistry and Physics, 32nd Edition (Chemical Rubber Publishing Company, Cleveland, Ohio, 1950), p. 1802.

19. S. Timoshenko and J. N. Goodier, Theory of Elasticity (McGraw-Hill Book Company, Inc., New York, 1951), p. 454.

20. R. T. Beyer and S. V. Letcher, Physical Ultrasonics (Academic Press, New London, 1969), pp. 23-30.

21. H. Kolsky, Stress Waves in Solids (Clarendon Press, Oxford, 1953), p. 79.

22. T. F. Hueter and R. H. Bolt, op. cit., p. 27.

23. L. E. Kinsler and A. R. Frey, Fundamentals of Acoustics (John Wiley and Sons, Inc., New York, 1950), p. 148.

24. E. E. Mikeska and C. M. McKinney, J. Acoust. Soc. Am. 56, 1418 (1974).

25. M. Greenspan and C. E. Tschiegg, J. Acoust. Soc. Am. 31, 75 (1959).

26. K. J. Diercks, Applied Research Laboratories Technical Report No. 72-18 (ARL-TR-72-18), Applied Research Laboratories, The University of Texas at Austin (1972), p. 8.

BIBLIOGRAPHY

Barnard, G. R., and C. M. McKinney, J. Acoust. Soc. Am. 33, 266 (1961).

Beyer, R. T., and S. V. Letcher, Physical Ultrasonics (Academic Press, New London, 1969), pp. 23-30.

Bowman, J. J., T. B. A. Senior, and P. L. E. Uslenghi, Electromagnetic and Acoustic Scattering by Simple Shapes (North-Holland Publishing Company, Amsterdam; John Wiley and Sons, Inc., New York, 1969).

Diercks, K. J., Applied Research Laboratories Technical Report No. 72-18 (ARL-TR-72-18), Applied Research Laboratories, The University of Texas at Austin (1972), p. 8.

Diercks, K. J., and T. G. Goldsberry, J. Acoust. Soc. Am. 35(A) (1963).

Diercks, K. J., T. G. Goldsberry, and C. W. Horton, Sr., J. Acoust. Soc. Am. 35, 59 (1963).

Diercks, K. J. K. McCormack, and D. B. James, J. Acoust. Soc. Am. 35, 59 (1963).

Diercks, K. J., K. McCormack, and D. B. James, J. Acoust. Soc. Am. 34, 1957 (1962). See also Appendix A of this report for wavelength calculations.

Faran, J. J., Jr., J. Acoust. Soc. Am. 23, 405 (1951).

Franz, W., and K. Deppermann, Ann. Physik. 10, 361 (1952).

Goldsberry, T. G., J. Acoust. Soc. Am. 42, 1298 (1967).

Greenspan, M., and C. E. Tschiegg, J. Acoust. Soc. Am. 31, 75 (1959).

Hodgeman, C. D., ed., Handbook of Chemistry and Physics, 32nd Edition (Chemical Rubber Publishing Company, Cleveland, Ohio, 1950), p. 1802.

Horton, C. W., Sr., J. Acoust. Soc. Am. 51, 1049 (1972).

Horton, C. W., Sr., W. R. King, and K. J. Diercks, J. Acoust. Soc. Am. 34, 1929 (1962).

Hueter, T. F., and R. H. Bolt, Sonics (John Wiley and Sons, Inc., New York, 1955) p. 28.

BIBLIOGRAPHY (Cont'd)

Kinsler, L. E., and A. R. Frey, Fundamentals of Acoustics (John Wiley and Sons, Inc., New York, 1950), p. 148.

Kolsky, H., Stress Waves in Solids (Clarendon Press, Oxford, 1953), p. 79.

Mikeska, E. E., and C. M. McKinney, J. Acoust. Soc. Am. 56, 1418 (1974).

Morse, P. M., Vibration and Sound (McGraw-Hill Book Company, Inc., New York, 1936).

Lord Rayleigh, Theory of Sound (Dover Publications, New York, 1945).

Roark, R. J., Formulas for Stress and Strain (McGraw-Hill Book Company, Inc., New York, 1965), p. 416.

Timoshenko, S., and J. N. Goodier, Theory of Elasticity (McGraw-Hill Book Company, Inc., New York, 1951).

Wood, Alexander, Acoustics (Dover Publications, Inc., 1966), p. 74.

16 May 1977

DISTRIBUTION LIST FOR
ARL-TR-77-28
UNDER CONTRACT N00024-75-C-6078, Item 0004
UNCLASSIFIED

Copy No.

Commander
Naval Sea Systems Command
Department of the Navy
Washington, DC 20362

1 Attn: D. E. Porter (Code 06H1-11)
2 Code 660F
3 Code 660C
4 Code 661C
5 Code 660E
6 Code 06H1-B
7 Code 06H2
8 Code 06H4
9 - 10 Technical Library (Code 09G32)

11 Chief of Naval Research
Department of the Navy
Ocean Science Program
Target Physics Workshop
Arlington, VA 22217
Attn: F. P. Diemer
Research/Planning Coordinator

12 Director
Naval Research Laboratory
Department of the Navy
Washington, DC 20390

Commander
Naval Ocean Systems Center
San Diego, CA 92132
13 Attn: R. Bolam
14 Library

Officer in Charge
New London Laboratory
Naval Underwater Systems Center
New London, CT 06320
15 Attn: H. Newman
16 R. Chapman
17 Library

Dist. List for ARL-TR-77-28 under Contract N00024-75-C-6078, Item 0004 (Cont'd)

Copy No.

18 — David Taylor Naval Ship Research and Development Center
Department of the Navy
Bethesda, MD 20084

Commanding Officer
Naval Coastal Systems Laboratory
Panama City, FL 32401
19 — Attn: Glenn McLeroy
20 — Rolf Mossbacher

21 — Commanding Officer
Naval Air Development Center
Johnsville
Warminster, PA 18974

22 — Office of the Director of Defense
Research and Engineering
The Pentagon
Washington, DC 20301

23 - 24 — Commanding Officer
Naval Surface Weapons Center
White Oak Laboratory
Department of the Navy
Silver Spring, MD 20910

25 - 36 — Commanding Officer
Defense Documentation Center
Defense Services Administration
Cameron Station, Building 5
5010 Duke Street
Alexandria, VA 22314

37 — Office of Naval Research
Resident Representative
Room 582, Federal Building
Austin, TX 78701

38 — General Dynamics
Electric Boat Division
Eastern Point Road
Groton, CT 06340
Attn: William H. Ezzell

Dist. List for ARL-TR-77-28 under Contract N00024-75-C-6078, Item 0004 (Cont'd)

Copy No.

39	Southwest Research Institute P. O. Drawer 28510 San Antonio, TX 78228 Attn: Dr. George Gruber
40	Sonar Development Division, ARL/UT
41	Klaus W. Alkier, ARL/UT
42	Garland R. Barnard, ARL/UT
43	Hollis Boehme, ARL/UT
44	K. Jerome Diercks, ARL/UT
45	Marshall E. Frazer, ARL/UT
46	Tommy G. Goldsberry, ARL/UT
47	Loyd D. Hampton, ARL/UT
48	James E. Stockton, ARL/UT
49	Reuben H. Wallace, ARL/UT
50	Joseph H. Willman, ARL/UT
51	Charles L. Wood, ARL/UT
52	Library, ARL/UT
53 - 57	Reserve, ARL/UT